NASA TECHNICAL NOTE

NASA TN D-7071

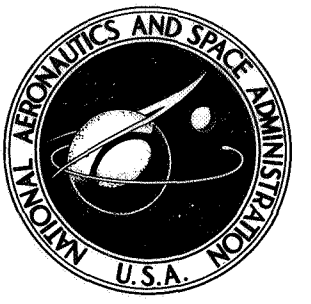

NASA TN D-7071

LOW-SPEED AERODYNAMIC CHARACTERISTICS OF AN AIRFOIL OPTIMIZED FOR MAXIMUM LIFT COEFFICIENT

by

Gene J. Bingham

Langley Directorate,
U.S. Army Air Mobility R&D Laboratory
Hampton, Va. 23365

and

Allen Wen-shin Chen

Langley Research Center
Hampton, Va. 23365

NATIONAL AERONAUTICS AND SPACE ADMINISTRATION • WASHINGTON, D. C. • DECEMBER 1972

1. Report No.	2. Government Accession No.	3. Recipient's Catalog No.
NASA TN D-7071		

4. Title and Subtitle	5. Report Date
LOW-SPEED AERODYNAMIC CHARACTERISTICS OF AN AIRFOIL OPTIMIZED FOR MAXIMUM LIFT COEFFICIENT	December 1972
	6. Performing Organization Code

7. Author(s)	8. Performing Organization Report No.
Gene J. Bingham (Langley Directorate, U.S. Army Air Mobility R&D Laboratory) and Allen Wen-shin Chen (Langley Research Center)[1]	L-8491
	10. Work Unit No. 501-06-05-02
9. Performing Organization Name and Address	11. Contract or Grant No.
NASA Langley Research Center Hampton, Va. 23365	
	13. Type of Report and Period Covered
12. Sponsoring Agency Name and Address	Technical Note
National Aeronautics and Space Administration Washington, D.C. 20546	14. Sponsoring Agency Code

15. Supplementary Notes

[1]NRC-NASA Resident Research Associate

16. Abstract

An investigation has been conducted in the Langley low-turbulence pressure tunnel to determine the two-dimensional characteristics of an airfoil optimized for maximum lift coefficient. The design maximum lift coefficient was 2.1 at a Reynolds number of 9.7×10^6. The airfoil with a smooth surface and with surface roughness was tested at angles of attack from -6° to 26°, at Reynolds numbers (based on airfoil chord) from 2.0×10^6 to 12.9×10^6, and at Mach numbers from 0.10 to 0.35. The experimental results are compared with values predicted by theory.

The experimental pressure distributions observed at angles of attack up to at least 12° were similar to the theoretical values except for a slight increase in the experimental upper-surface pressure coefficients forward of 26 percent chord and a more severe gradient just behind the minimum-pressure-coefficient location. The maximum lift coefficients were measured with the model surface smooth and, depending on test conditions, varied from 1.5 to 1.6 whereas the design value was 2.1.

17. Key Words (Suggested by Author(s))	18. Distribution Statement
Airfoil Airfoil design Wind-tunnel testing	Unclassified – Unlimited

19. Security Classif. (of this report)	20. Security Classif. (of this page)	21. No. of Pages	22. Price*
Unclassified	Unclassified	53	$3.00

*For sale by the National Technical Information Service, Springfield, Virginia 22151

LOW-SPEED AERODYNAMIC CHARACTERISTICS OF AN AIRFOIL OPTIMIZED FOR MAXIMUM LIFT COEFFICIENT

By Gene J. Bingham and Allen Wen-shin Chen*
Langley Research Center

SUMMARY

An investigation has been conducted in the Langley low-turbulence pressure tunnel to determine the two-dimensional characteristics of an airfoil optimized for maximum lift coefficient. The design maximum lift coefficient was 2.1 at a Reynolds number of 9.7×10^6. The airfoil with a smooth surface and with surface roughness was tested at angles of attack from -6^o to 26^o, at Reynolds numbers (based on airfoil chord) from 2.0×10^6 to 12.9×10^6, and at Mach numbers from 0.10 to 0.35. The experimental results are compared with values predicted by theory.

The experimental pressure distributions observed at angles of attack up to at least 12^o were similar to the theoretical values except for a slight increase in the experimental upper-surface pressure coefficients forward of 26 percent chord and a more severe gradient just behind the minimum-pressure-coefficient location. The maximum lift coefficients were measured with the model surface smooth and, depending on test conditions, varied from 1.5 to 1.6 whereas the design value was 2.1. With roughness at 25 percent chord, the maximum lift coefficient decreased to about 1.4. With roughness at the leading edge, the maximum lift coefficients decreased to as low as 1.3 and 0.8 (depending on Reynolds number). Even though the boundary layer at the tunnel-wall—airfoil juncture separated prior to stall and thereby limited the maximum lift coefficient developed, the design value could not be achieved because of viscous effects. At Mach numbers from 0.24 to 0.35, the angle-of-attack range for a linear lift curve and the maximum lift coefficient were less than those measured at lower Mach numbers. The experimental and theoretical pitching-moment coefficients are in good agreement for the linear part of the curves.

INTRODUCTION

Airfoils with high maximum lift coefficients are desirable for airplanes designed with short take-off and landing run capability. Accordingly, leading-edge slats and/or

---

*NRC-NASA Resident Research Associate.

trailing-edge flaps are commonly used to extend the maximum-lift range of conventional airfoils. An analytical airfoil design method has been defined by references 1 and 2 to obtain high maximum lift coefficients for single-element or multiple-element airfoils. The method first determines the separation-free pressure distribution at maximum lift and, based on this pressure distribution, determines the airfoil coordinates for an incompressible-inviscid flow. The separation-free pressure distribution is based on the criteria of references 3 and 4 and results in zero skin friction in the pressure-recovery region of the airfoil.

An experimental investigation has been conducted to evaluate the analytical design method by providing a comparison between theoretical and experimental aerodynamic characteristics of a single-element airfoil. The airfoil was designed to have a maximum lift coefficient of 2.1 at a Reynolds number (based on airfoil chord) of 9.7×10^6.

The tests were conducted in the Langley low-turbulence pressure tunnel at Mach numbers from 0.10 to 0.35 and at Reynolds numbers (based on airfoil chord) from 2.0×10^6 to 12.9×10^6. The model was tested smooth and with two fixed-transition configurations. Lift and pitching-moment coefficients were determined from measurements of airfoil-surface static pressures.

SYMBOLS

The units used for the physical quantities of this paper are given both in the International System of Units (SI) and in the U.S. Customary Units. The measurements and calculations were made in the U.S. Customary Units.

C_p pressure coefficient, $\dfrac{p_{local} - p_\infty}{q_\infty}$

c chord of airfoil, cm (in.)

c_c section chord-force coefficient, $\displaystyle\int_{\text{Forward } (t/c)_{max}} C_p \, d\left(\frac{z}{c}\right) - \int_{\text{Aft } (t/c)_{max}} C_p \, d\left(\frac{z}{c}\right)$

c_n section normal-force coefficient, $\displaystyle\int_{\text{Lower surface}} C_p \, d\left(\frac{x}{c}\right) - \int_{\text{Upper surface}} C_p \, d\left(\frac{x}{c}\right)$

c_m section pitching-moment coefficient about 0.25c, $\displaystyle\oint C_p \left(\frac{z}{c}\right) d\left(\frac{z}{c}\right) + \oint C_p \left(\frac{x}{c} - 0.25\right) d\left(\frac{x}{c}\right)$

c_l section lift coefficient, $c_n(\cos \alpha) - c_c(\sin \alpha)$

M	free-stream Mach number
p	static pressure, N/m^2 (lb/ft^2)
q	dynamic pressure, N/m^2 (lb/ft^2)
R	Reynolds number (based on free-stream conditions and airfoil chord)
t	airfoil thickness, cm (in.)
V	velocity, m/s (fps) (see fig. 1)
x	airfoil abscissa, cm (in.) (see fig. 1)
y	spanwise distance from airfoil plane of symmetry, cm (in.)
z	airfoil ordinate, cm (in.) (see fig. 1)
α	angle of attack of airfoil, angle between reference line and airstream axis, deg (see fig. 1)

Subscripts:

max	maximum
min	minimum
∞	undisturbed stream conditions

AIRFOIL DESIGN

The airfoil (fig. 1) was designed by the incompressible-inviscid method of reference 2 to have a $c_{l,max}$ of 2.1 at a Reynolds number (based on airfoil chord) of 9.7×10^6. The design problem was treated in two steps: The first step defines the pressure distribution at $c_{l,max}$ and the second step determines the corresponding airfoil coordinates via an iteration procedure.

The final design pressure distributions for both upper and lower surfaces are given graphically in figure 2. The design upper-surface pressure distribution (at $\alpha = 18.35^o$)

incorporated (1) an abrupt pressure decrease from the stagnation pressure to a prescribed minimum pressure value, (2) a pressure plateau, and (3) a rise in pressure from the plateau value to a selected trailing-edge value. The minimum pressure coefficient, the length of the plateau, and the shape of the pressure rise are optimized by the design method. The pressure rise is designed to provide zero skin friction everywhere in the pressure-recovery region but with no separation; therefore, any further attempt to increase lift coefficient (which in consequence steepens the adverse pressure gradient) would cause boundary-layer separation. The expression for such a pressure recovery has been defined and experimentally verified by Stratford (refs. 3 and 4). In applying Stratford's criteria for the present design, a turbulent boundary layer was assumed to exist along the entire upper surface of the airfoil. The initial lower-surface pressure distribution was arbitrarily selected to be near linear from the stagnation pressure to the selected trailing-edge value.

After the pressure distribution was defined, an airfoil geometry that would generate the distribution was obtained by using Sato's incompressible-inviscid conformal transformation method (ref. 5). The resulting airfoil was highly cambered and had a maximum thickness of only 6 percent chord. This thickness was considered too small from a structural viewpoint; therefore, the thickness was arbitrarily increased by smooth fairing of the lower surface from near the leading edge to the trailing edge. The resulting airfoil had a thickness of about 12 percent chord. The thickened airfoil naturally did not have the initially defined upper-surface velocity distribution. The maximum deviation was 0.15 of free-stream velocity. Hence, this airfoil had to be modified by the iteration procedure of reference 2 so that the upper-surface velocity distribution could be restored. The iteration procedure of reference 2 computes the incompressible-inviscid velocity distribution on a given airfoil by using Oellers' method (ref. 6) and modifies the airfoil coordinates according to the difference between the computed velocity distribution and the desired velocity distribution. The modification was repeated five times until the computed and desired velocity distributions agreed to the third decimal place. The maximum change of geometry introduced during the iteration was 0.5 percent chord. The angle of attack, which was measured from the original zero-lift line (fig. 1), was maintained at 18.35° during the procedure. After the airfoil shape was defined, the pressure distribution was computed at selected angles of attack (fig. 2) by the same computer program.

APPARATUS AND PROCEDURE

Model Description

The airfoil coordinates defined by the design procedure are presented in table I. The maximum airfoil thickness was about 12.5 percent chord and was located at approximately 0.25c.

The model was machined from a solid aluminum billet and had a smooth polished surface. The chord was 60 cm (23.62 in.) and the span was 91.44 cm (36 in.). Figure 3 shows several photographs of the model mounted in the wind tunnel. The airfoil was equipped with 35 upper-surface and 29 lower-surface orifices at midspan and 18 upper-surface orifices distributed between midspan and the right-hand (looking upstream) tunnel wall. The orifice locations are indicated in table II and are shown in figure 4. All orifices were drilled perpendicular to the local surface with a drill diameter of 0.813 mm (0.032 in.).

Wind Tunnel and Model Support

The Langley low-turbulence pressure tunnel (ref. 7) is a closed-throat single-return tunnel which can be operated at stagnation pressures from 1 to 10 atm (1 atm = 101.325 kN/m^2). At 1 atm the attainable Mach number and Reynolds number are 0.46 and 6.6×10^6 per m (2.0×10^6 per ft), respectively; at 10 atm the corresponding values are 0.23 and 49×10^6 per m (15×10^6 per ft). The test section is 0.9144 m (3 ft) wide by 2.286 m (7.5 ft) high.

Circular end plates provide attachments for the two-dimensional models (figs. 3 and 4). The end plates are 101.6 cm (40 in.) in diameter, are flush with the tunnel wall, and are hydraulically rotated to provide for model-angle-of-attack changes. The model was mounted so that the center of rotation of the circular plates was at 0.25c on the reference line (shown in fig. 1). The air gap at the tunnel walls was sealed.

Instrumentation

Measurements included pressures and angles of attack. The measurements of the airfoil-surface static and wake-rake pressures were made by an automatic pressure-scanning system. Pressure transducers with different pressure ranges were used to measure the pressures in different regions. The selection was based on the anticipated pressures, and transducers with ranges of ±69, ±34, and ±17 kN/m^2 (±10, ±5, and ±2.5 psi) were used. The ±69-kN/m^2 (±10-psi) transducer was used from the leading edge to 0.35c on the upper surface and to 0.05c on the lower surface. The ±34-kN/m^2 (±5-psi) transducer was used from 0.37c to 0.55c on the upper surface. The ±17-kN/m^2 (±2.5-psi) transducer was used on the remainder of the airfoil. Basic tunnel pressures (stagnation pressure and stagnation pressure minus reference static pressure) were measured with precision pressure transducers. Angle of attack was determined from the output of a calibrated potentiometer attached to the circular end plates which supported the model.

Test

For the tests, the free-stream Mach number ranged from 0.10 to 0.35, and the Reynolds numbers (based on airfoil chord) ranged from 2.0×10^6 to 12.9×10^6. The

geometric angle of attack, which is the angle between the airfoil reference line (fig. 1) and the free stream, was varied from about -6° to 26°. The model was tested with smooth polished surfaces and with two different roughness strips to induce boundary-layer transition. One roughness configuration was a narrow strip applied full span to the airfoil upper surface rearward of the 0.25c station for a distance of 3.175 mm (0.125 in.). It was sized according to the method described in reference 8 and consisted of 0.279-mm-diameter (0.011-in.) carborundum grains. The other roughness configuration was a wide strip like the standard roughness described in reference 9. It had the same grain size as that used for the narrow strip (0.279 mm) and was applied to both the upper and lower airfoil surfaces at the leading edge over a surface length equal to 0.08c measured from the leading edge. In both cases, the grains were thinly spread to cover 5 to 10 percent of the strip surface area and were attached to the surface with lacquer. In addition, the smooth airfoil was tested with a mixture of oil and lampblack brushed on the surface to define surface streamline patterns at angles of attack near stall. For the oil-flow tests, angle of attack was varied from about 12.3° to 20.0° and the results were recorded on a video tape.

Data Reduction and Accuracy

The airfoil-surface static-pressure measurements were reduced to standard pressure coefficients and then integrated by using a trapezoidal rule to obtain section normal-force, chord-force, and pitching-moment coefficients. The pitching-moment coefficients were referenced to 0.25c on the airfoil reference line, and the lift coefficients were obtained by resolving the normal- and chord-force coefficients perpendicular to the free stream. Airfoil wake pressures were obtained with a wake-survey rake but the unsteadiness of the wake at all angles of attack precluded an accurate determination of drag by this method. Therefore, drag-coefficient data are not presented. The data indicate that surface static pressures were not influenced by the unsteadiness of the wake.

The maximum error in pressure measurement which could occur is 0.25 percent, full-scale, for each pressure transducer. This results in C_p errors of ±0.090, ±0.045, and ±0.023 for the ±69-, ±34-, and ±17-kN/m^2 (±10-, ±5-, and ±2.5-psi) pressure transducers, respectively, at the lowest dynamic pressure.

Hand fairing of three representative types of pressure distributions and subsequent integrations by planimeter for c_c, c_n, and $c_{m,\text{leading edge}}$ have been compared with trapezoidal rule numerical integrations, and the maximum errors found were 0.006, 0.004, and 0.001, respectively. When these errors are included in c_l and c_m, the errors are 0.004 and 0.001, respectively.

The standard low-speed wind-tunnel boundary corrections obtained by using the method of reference 10 were less than 2 percent of the computed coefficients, which is within the accuracy of the data sampling, and therefore not applied.

PRESENTATION OF RESULTS

The results of this investigation have been reduced to coefficient form and are presented in figures 5 to 16. An outline of the data figures is as follows:

DISCUSSION

Oil-Flow Patterns and Spanwise Pressure Distributions

Oil-flow patterns and upper-surface spanwise static-pressure distributions provided an indication of the two-dimensionality of the flow over the airfoil model. Pressure distributions at $\frac{x}{c} = 0.40$, 0.65, and 0.90 are presented in figure 5 to assist in assessing the flow conditions on the model. With the smooth surface (fig. 5(a)), the near-uniform distribution (and two-dimensional flow) disappeared at angles of attack between about 16.1^{o} and 18.7^{o}. This result is consistent with the oil-flow patterns observed at

$R = 2.0 \times 10^6$ with the smooth airfoil. The oil-flow traces indicated two-dimensional flow at angles of attack as high as 17^o. However, at the next angle setting, $\alpha = 18.4^o$, figure 6 clearly showed that the boundary layer was separated from the airfoil and tunnel wall at the airfoil-wall juncture prior to separation inboard of the juncture. The flow in the juncture region first moved upstream, then moved toward the center line, and finally moved downstream in the airfoil center-line region. The loss in two-dimensionality with the onset of separation was observed in reference 11 also. The spanwise pressure coefficients (figs. 5(b) and (c)) indicate that two-dimensionality is lost at angles of attack between about 12.1^o and 16.2^o with roughness at 0.25c and at the leading edge. Because of the three-dimensional flow, the interpretation of the absolute aerodynamic coefficients at the highest angle of attack is open to some question.

Chordwise Pressure Distributions

The chordwise static-pressure distributions of the airfoil model with a smooth surface at angles of attack from about 0^o to 21.5^o and at Reynolds numbers (based on airfoil chord) from 3.0×10^6 to 12.8×10^6 are presented in figure 7. The minimum upper-surface pressure coefficient is generally located near 0.26c at angles of attack up to about 16^o and a Reynolds number of 3.0×10^6, and a pressure plateau tends to develop forward of $C_{p,min}$ as angle of attack is increased from about 0^o to 16^o. At Reynolds numbers of 5.7×10^6 and 9.3×10^6, these characteristics appear up to an angle of attack of 18^o but they may not represent purely two-dimensional results because of flow separation at the tunnel wall. The favorable pressure gradient up to 0.26c probably permitted laminar flow over much of this region. From about 0.26c to 0.38c, a large upper-surface adverse pressure gradient is indicated. The gradient continues to the trailing edge at a reduced rate at angles of attack from about 0^o to 16^o. At angles of attack of about 18.6^o and 21.5^o, separation is indicated by the regions of uniform pressures and/or by the nonuniform spanwise distribution (fig. 5(a)).

When roughness was added to the upper surface at 0.25c, the pressure distributions (fig. 8) are similar to those for the smooth-surface configurations. However, the angle of attack at which separation was first indicated decreased about 2^o; the actual value depended on Reynolds number. This decrease apparently results from a destabilizing effect on the boundary-layer velocity profile at the beginning of the adverse-pressure-gradient region where the roughness is located. When the leading-edge roughness was applied (fig. 9), the angle of attack for separation again decreased, apparently for the same reason. In this case, separation at $\alpha = 12.2^o$ was eliminated by increasing the Reynolds number from 2.9×10^6 to 5.6×10^6 and thereby decreasing the boundary-layer thickness.

Experimentally measured and theoretically predicted pressure distributions at three angles of attack are presented in figure 10 for $R \approx 9 \times 10^6$. Both inviscid and viscous

theoretical pressure distributions were obtained by using the approach of reference 12. The inviscid solution of reference 12 is identical to that used in reference 2. The angles of attack are near those considered in the design analysis (see fig. 2). At $\alpha \approx 3^{\circ}$, the respective experimental and theoretical curves are in general agreement on both upper and lower surfaces although the adverse pressure gradient immediately behind the minimum pressure coefficient was measured to be more severe than predicted by theory. At $\alpha \approx 12^{\circ}$, the curves also agree reasonably well except for a slight increase in the experimental upper-surface pressure forward of 0.26c and, again, a more severe gradient just behind the minimum-pressure-coefficient location. This steeper adverse pressure gradient observed in the investigation may explain the near-zero skin friction which occurred below the design angle of attack. The attainment of near-zero skin friction was confirmed by the oil-flow traces (not presented herein). At $\alpha \approx 18^{\circ}$, boundary-layer separation caused substantial differences between experimental and theoretical pressure coefficients on both upper and lower surfaces. As noted previously, the $\alpha \approx 18^{\circ}$ data may not represent purely two-dimensional results because of the flow separation at the tunnel wall.

Section Lift Characteristics

The section lift characteristics of the airfoil model with a smooth surface are presented in figure 11(a). The lift-curve slope at zero lift was measured to be about 0.093 per deg at $R = 3.0 \times 10^6$ and increased to 0.102 per deg for $R \geq 5.7 \times 10^6$. The angle of attack for zero lift (1.2°) was approximately the same value at all test Reynolds numbers. The maximum lift coefficient increased only from about 1.5 to 1.6 as Reynolds number was increased from 3.0×10^6 to 9.2×10^6 (apparently due to the usual reduction in boundary-layer thickness with increasing Reynolds number) and then remained near constant (≈ 1.6) as Reynolds number was increased to 12.8×10^6. As previously noted, test results following separation (and stall) may not represent truly two-dimensional data.

The addition of the transition strip to the upper surface at 0.25c only influenced $c_{l,max}$ (see fig. 11(b)); that is, the value of $c_{l,max}$ was about 1.4 at all Reynolds numbers or about 0.1 to 0.2 less than that for the smooth airfoil. With roughness distributed from the leading edge to 0.08c measured along the surface, the value of $c_{l,max}$ (fig. 11(c)) decreased to about 0.8 at the lowest Reynolds number (2.9×10^6) and to 1.3 at a Reynolds number of 12.8×10^6. Also, the lift-curve slope again increased abruptly as Reynolds number was increased from 2.9×10^6 to 5.6×10^6. The influences of Reynolds number on lift-curve slope along with the measured adverse pressure gradient aft of 0.26c (which is stronger than that of the inviscid case) suggest that the design method should incorporate a more complete boundary-layer analysis, at least in the final iteration.

Experimental and theoretical lift coefficients are presented in figure 12 for $R \approx 9 \times 10^6$, which is near the design value of 9.7×10^6. The inviscid case was computed by the approach of reference 6, which was incorporated into the computer program of reference 2. The viscous cases (smooth airfoil, roughness at 0.25c, and roughness at leading edge) are computed by the approach of reference 12. As would be expected, the computed lift-curve slopes decrease as the viscous influences increase. Of course, the inviscid case is separation free but the viscous solutions indicate the onset of separation as follows: 21.5° with the smooth surface, 21.5° with transition fixed at 0.25c on the upper surface, and 18.1° with transition fixed at the leading edge. The slopes of the experimental lift curves for the three airfoil surface conditions are about equal to zero lift but are below those predicted by reference 12. More significant, however, are the differences in $c_{l,max}$ and the angle of attack for $c_{l,max}$. For the smooth airfoil, the value of the experimental $c_{l,max}$ at $\alpha = 16.6^\circ$ is about 0.2 below the inviscid or design value (1.6 compared with 1.8) and the angle of attack for $c_{l,max}$ is about 5° below the angle of attack for first separation for the viscous solution ($\alpha = 16.6^\circ$ compared with 21.5°). Part of the difference probably results from the previously discussed separation at the airfoil-wall juncture and the associated deviation from two-dimensional flow. However, the results obtained with the three airfoil surface conditions indicate that viscous effects at angles of attack below initial separation are significantly greater than those predicted by reference 12. Realizing that reference 6 (and ref. 2) deals with inviscid flows only, it is not surprising that the design $c_{l,max}$ of 2.1 was not achieved. But, the value of $c_{l,max}$ would probably be higher than that of figure 11(a) (perhaps 1.8 obtained by extrapolating the c_l curve to the design angle of attack, 18.35°) if the wind-tunnel flow had remained two-dimensional up to airfoil stall.

Although a comparison of experiment with incompressible-inviscid theory was the primary interest of the investigation, data were obtained to examine some of the influence of free-stream Mach number on the maximum lift coefficient. For these tests, the Reynolds number (based on airfoil chord) was approximately 3.5×10^6, and the Mach number range (0.10 to 0.35) was defined by the tunnel operational envelope. The pressure-coefficient data are not presented but they were similar to those of figure 7. An analysis of all the pressure coefficients indicated that the local flow was subsonic at all test Mach numbers and angles of attack, and, as previously discussed, the tunnel flow remained two-dimensional only for the linear portion of the lift curves. (See fig. 13.) At Mach numbers from 0.24 to 0.35, the angle-of-attack range for a linear lift curve and the $c_{l,max}$ were less than those measured at the lower Mach numbers. The reasons for this trend are not apparent but it may be related to the loss in two-dimensionality of the tunnel flow.

Section Pitching-Moment Characteristics

The section pitching-moment data (fig. 14) indicate coefficients from about -0.04 to 0.01 for angles of attack from about 0° to 16° for the airfoil with the smooth surface and with surface roughness at 0.25c. With roughness at the leading edge, the angle-of-attack range for approximately the same c_m values was about 0° to 10°. A comparison of experimental and theoretical viscous solutions of reference 12 (fig. 15) indicates good agreement for the linear part of the curves. The influence of Mach number on pitching moment (fig. 16) is consistent with the previous discussion in the section on lift characteristics; that is, at Mach numbers from 0.24 to 0.35, the angle-of-attack range for a linear pitching-moment curve is about 1° less than that at the lower Mach number.

CONCLUSIONS

An investigation has been conducted in the Langley low-turbulence pressure tunnel to evaluate the two-dimensional characteristics of an airfoil optimized for maximum lift coefficient. The design maximum lift coefficient was 2.1 at a Reynolds number of 9.7×10^6. The airfoil with a smooth surface and with surface roughness was tested at angles of attack from -6° to 26°, at Reynolds numbers (based on airfoil chord) from 2.0×10^6 to 12.9×10^6, and at Mach numbers from 0.10 to 0.35. The experimental results were compared with the theoretical design values and indicated the following conclusions:

1. The experimental pressure distributions observed at angles of attack up to at least 12° were similar to the theoretical values except for a slight increase in the experimental upper-surface pressure coefficients forward of 26 percent chord and a more severe gradient just behind the minimum-pressure-coefficient location. Near-zero skin friction was indicated in the region of the adverse pressure gradient by oil-flow traces.

2. The maximum measured lift coefficient varied from 1.5 to 1.6 for the airfoil with the smooth surface throughout the test Reynolds numbers range whereas the design value was 2.1. With roughness at the 25 percent chord, the maximum lift coefficient decreased to about 1.4. With roughness at the leading edge, the maximum lift coefficient was about 0.8 at a Reynolds number of 2.9×10^6 and 1.3 at a Reynolds number of 12.8×10^6.

3. The boundary layer at the tunnel-wall—airfoil juncture separated prior to separation inboard of the juncture and the wind-tunnel flow was no longer two-dimensional. The maximum lift coefficient probably could have been as much as 1.8 at the design angle of attack of 18.35° if the wind-tunnel flow had remained two-dimensional up to airfoil stall.

4. At Mach numbers from 0.24 to 0.35, the angle-of-attack range for a linear lift curve and the maximum lift coefficient were less than those measured at the lower Mach numbers.

5. The experimental and theoretical pitching-moment coefficients are in good agreement for the linear part of the curves.

Langley Research Center,
National Aeronautics and Space Administration,
Hampton, Va., October 30, 1972.

REFERENCES

1. Liebeck, Robert H.; and Ormsbee, Allen I.: Optimization of Airfoils for Maximum Lift. J. Aircraft, vol. 7, no. 5, Sept.-Oct. 1970, pp. 409-415.

2. Chen, Allen Wen-shin: The Determination of the Geometries of Multiple-Element Airfoils Optimized for Maximum Lift Coefficient. Ph.D. Thesis, Univ. of Illinois, 1971. (Available as TM X-67591.)

3. Stratford, B. S.: The Prediction of Separation of the Turbulent Boundary Layer. J. Fluid Mech., vol. 5, pt. 1, Jan. 1959, pp. 1-16.

4. Stratford, B. S.: An Experimental Flow With Zero Skin Friction Throughout Its Region of Pressure Rise. J. Fluid Mech., vol. 5, pt. 1, Jan. 1959, pp. 17-35.

5. Sato, Junzo: An Exact Two-Dimensional Incompressible Potential Flow Theory of Aerofoil Design With Specified Velocity Distributions. Trans. Japan Soc. Aeronaut. & Space Sci., vol. 9, no. 14, 1966, pp. 11-18.

6. Oellers, Heinz J.: Die Inkompressible Potentialströmung in der Ebenen Gitterstufe. Jahrb. 1962, WGLR, Friedr. Vieweg & Sohn (Braunschweig), pp. 349-353.

7. Von Doenhoff, Albert E.; and Abbott, Frank T., Jr.: The Langley Two-Dimensional Low-Turbulence Pressure Tunnel. NACA TN 1283, 1947.

8. Braslow, Albert L.; and Knox, Eugene C.: Simplified Method for Determination of Critical Height of Distributed Roughness Particles for Boundary-Layer Transition at Mach Numbers From 0 to 5. NACA TN 4363, 1958.

9. Abbott, Ira H.; Von Doenhoff, Albert E.; and Stivers, Louis S., Jr.: Summary of Airfoil Data. NACA Rep. 824, 1945.

10. Allen, H. Julian; and Vincenti, Walter G.; Wall Interference in a Two-Dimensional-Flow Wind Tunnel, With Consideration of the Effect of Compressibility. NACA Rep. 782, 1944. (Supersedes NACA WR A-63.)

11. Gregory, N.; Quincey, V. G.; O'Reilly, C. L.; and Hall, D. J.: Progress Report on Observations of Three-Dimensional Flow Patterns Obtained During Stall Development on Aerofoils, and on the Problem of Measuring Two-Dimensional Characteristics. C.P. No. 1146, Brit. A.R.C., 1971.

12. Stevens, W. A.; Goradia, S. H.; and Braden, J. A.: Mathematical Model for Two-Dimensional Multi-Component Airfoils in Viscous Flow. NASA CR-1843, 1971.

TABLE I.- DESIGN ORDINATES FOR AIRFOIL

[All dimensions in percent chord]

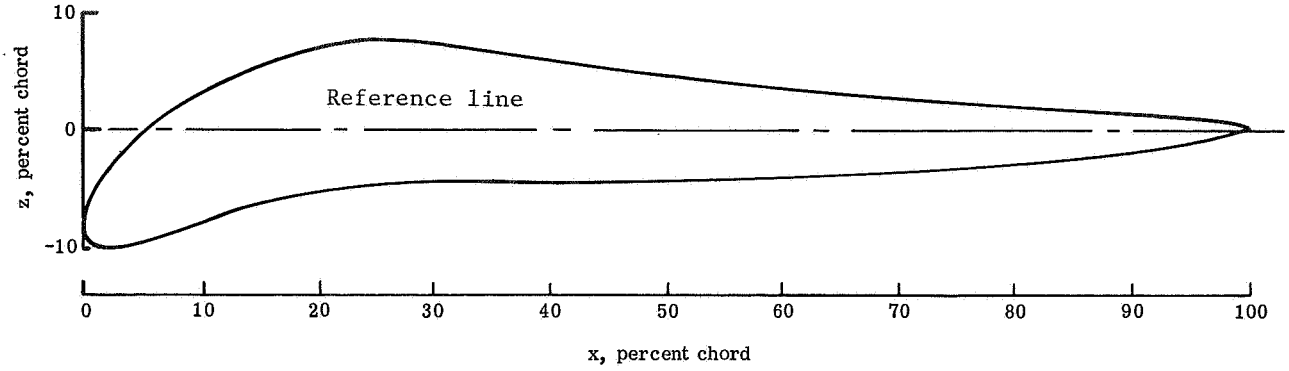

Station	Upper-surface ordinate	Station	Upper-surface ordinate
0.00	-8.41	40.66	6.08
.02	-8.23	44.05	5.63
.11	-7.55	47.54	5.19
.33	-6.77	51.10	4.75
.69	-5.91	54.71	4.33
1.19	-4.99	58.32	3.94
1.84	-4.03	61.92	3.57
2.60	-3.06	65.48	3.24
3.54	-2.03	68.97	2.93
4.61	-.99	72.37	2.66
5.82	.05	75.65	2.41
7.16	1.08	78.79	2.20
8.64	2.08	81.77	2.00
10.23	3.05	84.58	1.83
11.94	3.97	87.18	1.68
13.77	4.83	89.58	1.55
15.69	5.62	91.75	1.42
17.70	6.33	93.68	1.30
19.80	6.94	95.36	1.18
21.98	7.43	96.80	1.05
24.21	7.78	97.97	.90
26.49	7.94	98.87	.70
28.78	7.77	99.52	.63
31.32	7.35	99.87	.49
34.25	6.94	100.00	.40
37.38	6.51		

Station	Lower-surface ordinate	Station	Lower-surface ordinate
0.00	-8.41	45.68	-4.43
.05	-8.81	49.38	-4.35
.19	-9.24	53.00	-4.24
.42	-9.52	56.55	-4.14
.74	-9.72	60.02	-4.01
1.20	-9.85	63.41	-3.83
1.90	-9.90	66.72	-3.64
2.80	-9.86	69.94	-3.45
3.90	-9.68	73.09	-3.26
5.30	-9.35	76.12	-3.07
7.00	-8.84	79.01	-2.88
8.70	-8.28	81.77	-2.68
10.70	-7.68	84.38	-2.42
12.70	-7.07	86.81	-2.13
14.90	-6.40	89.11	-1.83
17.50	-5.75	91.24	-1.51
20.50	-5.17	93.15	-1.19
22.50	-4.88	94.87	-.87
26.50	-4.53	96.36	-.54
29.50	-4.41	97.60	-.24
32.50	-4.36	98.59	-.02
35.80	-4.36	99.32	.14
38.80	-4.40	99.81	.30
41.75	-4.44	100.00	.40

TABLE II.- SURFACE-ORIFICE LOCATIONS

[Locations given in percent airfoil chord]

(a) At center line

Upper-surface station	Lower-surface station
0.00	0.54
.35	1.02
.70	1.97
1.27	2.99
2.54	3.97
3.75	4.89
4.98	7.49
7.58	9.99
9.97	12.42
12.47	14.97
14.96	17.48
17.46	19.93
19.95	24.94
22.49	29.91
24.98	34.94
27.48	39.96
29.97	42.42
32.47	49.95
34.98	54.93
37.52	59.97
39.98	64.98
42.47	70.42
46.01	75.49
50.01	79.98
54.97	85.00
59.98	90.01
64.94	95.00
70.41	97.54
75.46	99.02
80.01	
84.94	
89.99	
94.98	
97.47	
98.99	

(b) Off center line (upper surface only)

Upper-surface station	Distance from center line					
40.00	12.70	25.40	38.10	50.80	63.50	72.00
65.00	12.70	25.40	38.10	50.80	63.50	72.00
90.00	12.70	25.40	38.10	50.80	63.50	72.00

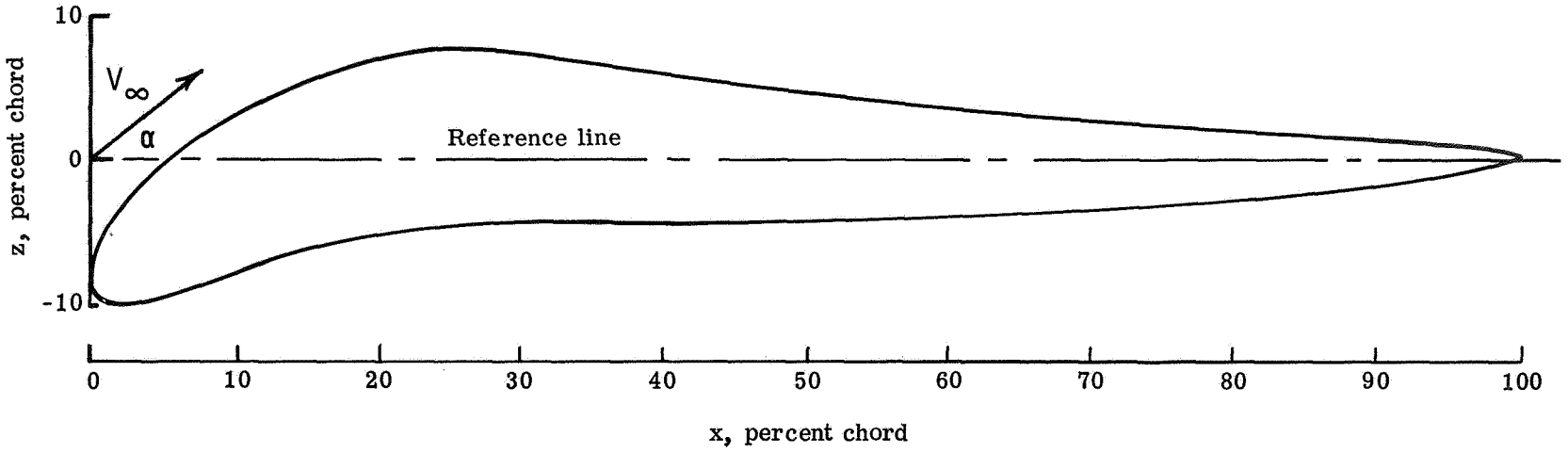

Figure 1.- Airfoil section shape.

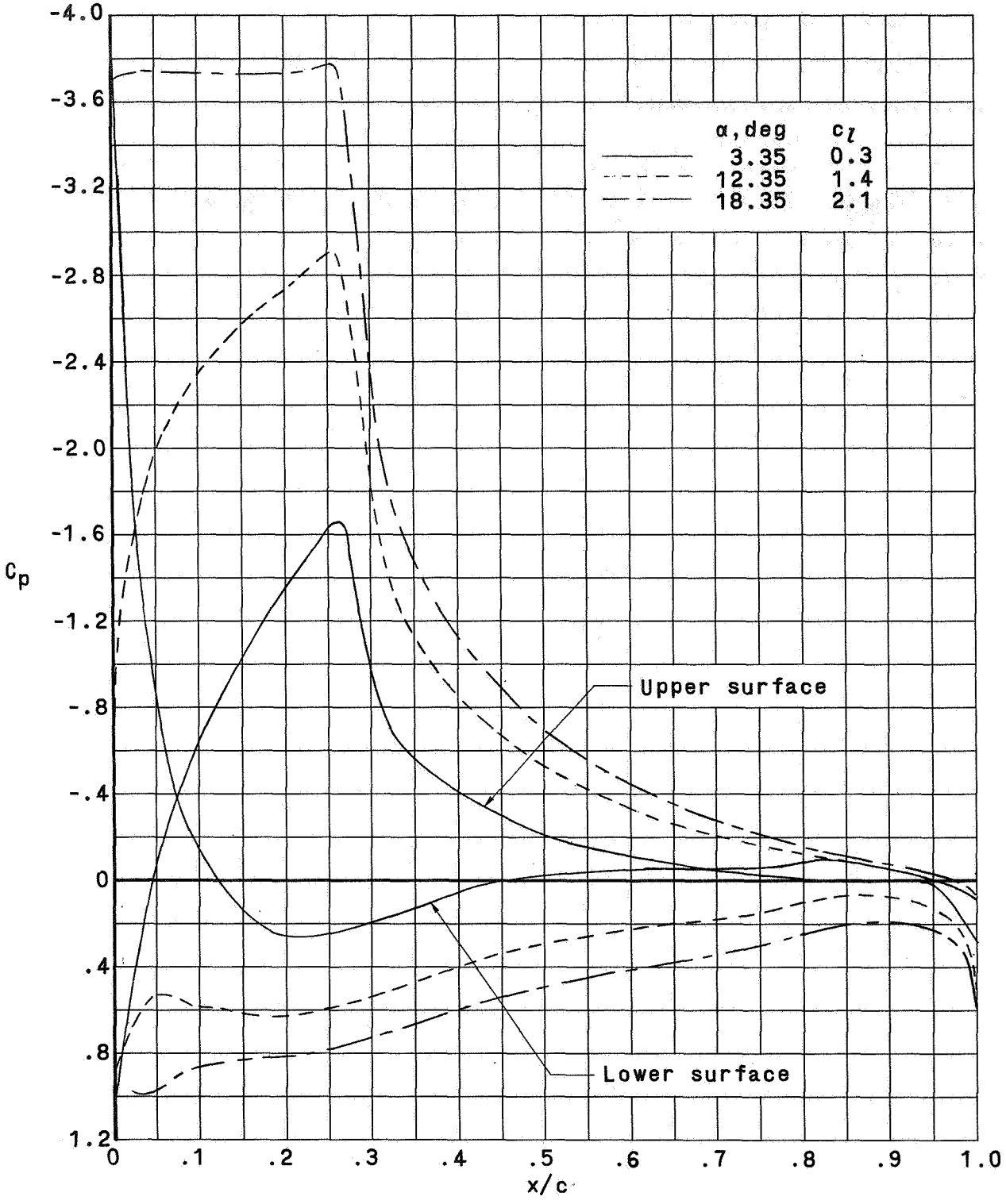

Figure 2.- Theoretical pressure distributions from reference 2. $R = 9.7 \times 10^6$.

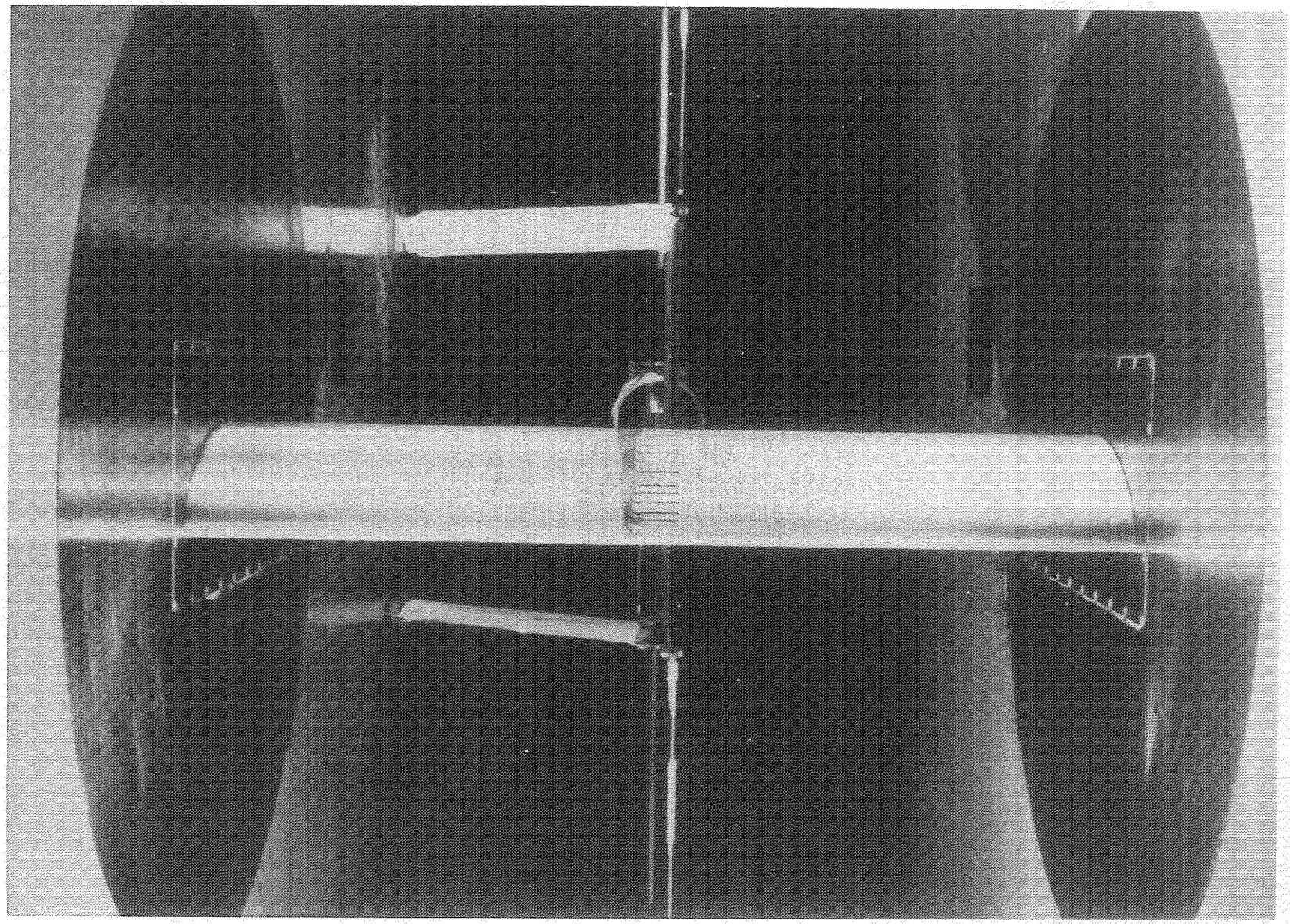

(a) Viewed from upstream, $\alpha = 0^{o}$. L-71-7066

Figure 3.- Photographs of airfoil mounted in wind tunnel.

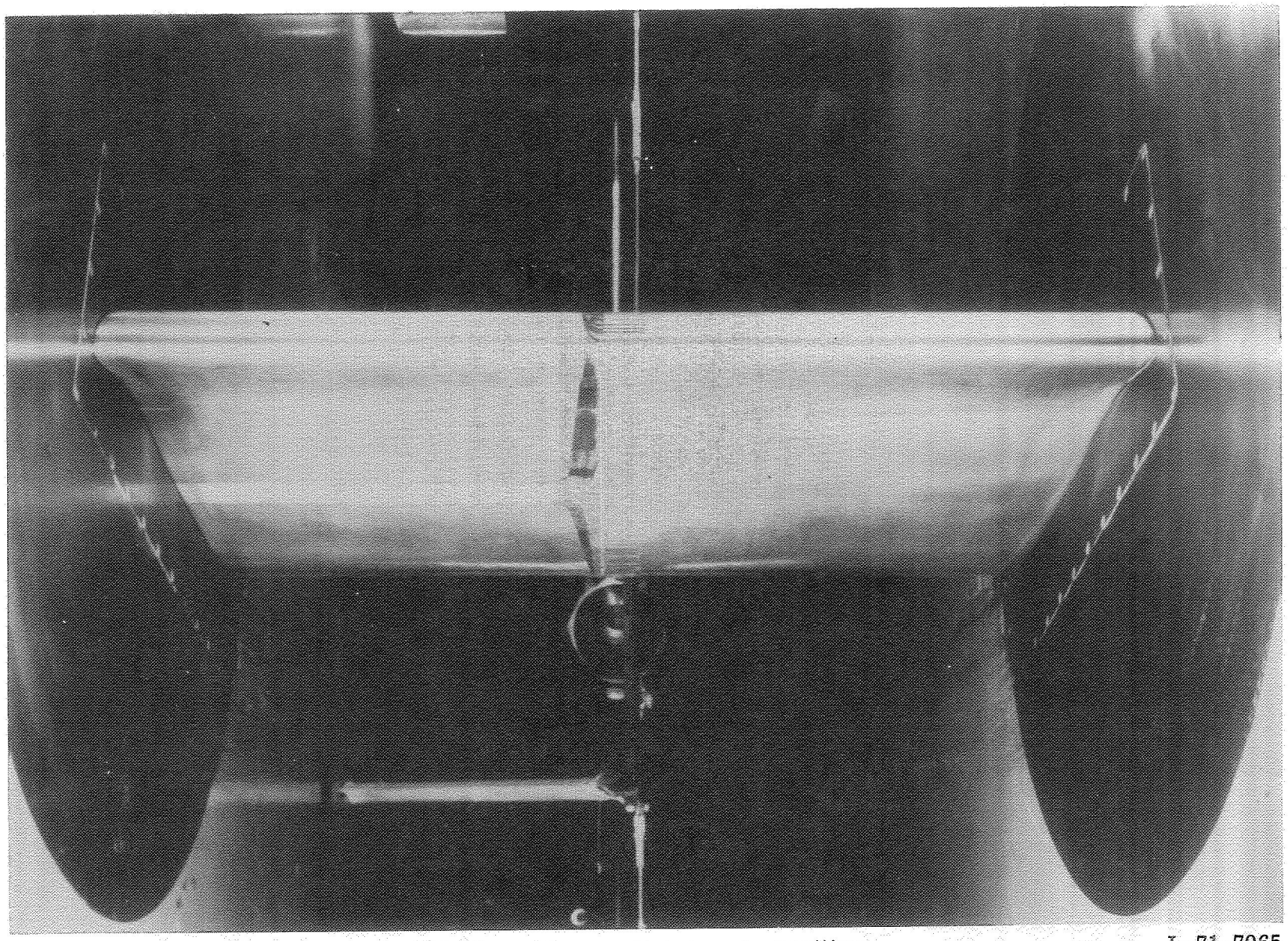

(b) Viewed from upstream, α positive. L-71-7065

Figure 3.- Continued.

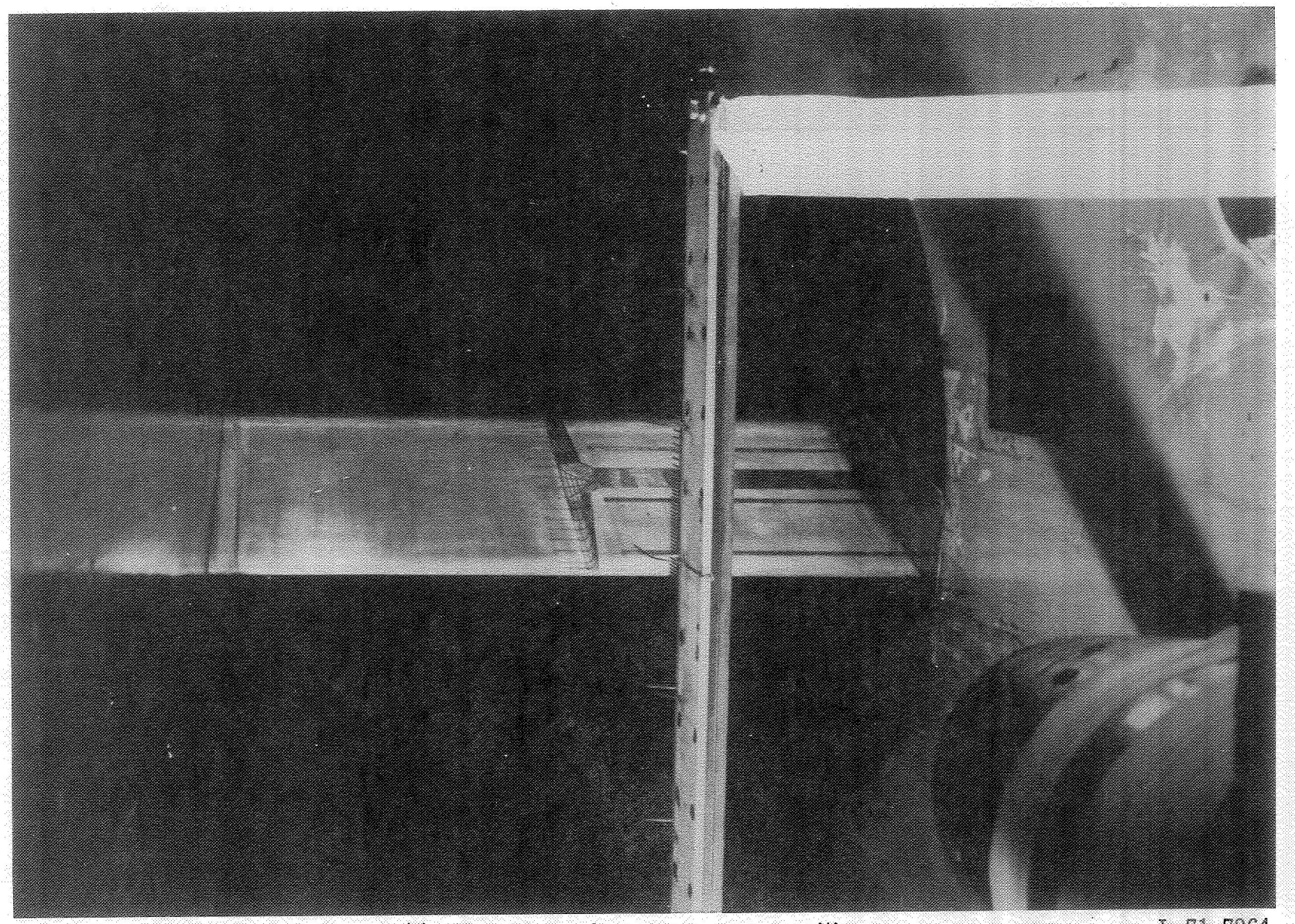

(c) Viewed from downstream, α positive. L-71-7064

Figure 3.- Concluded.

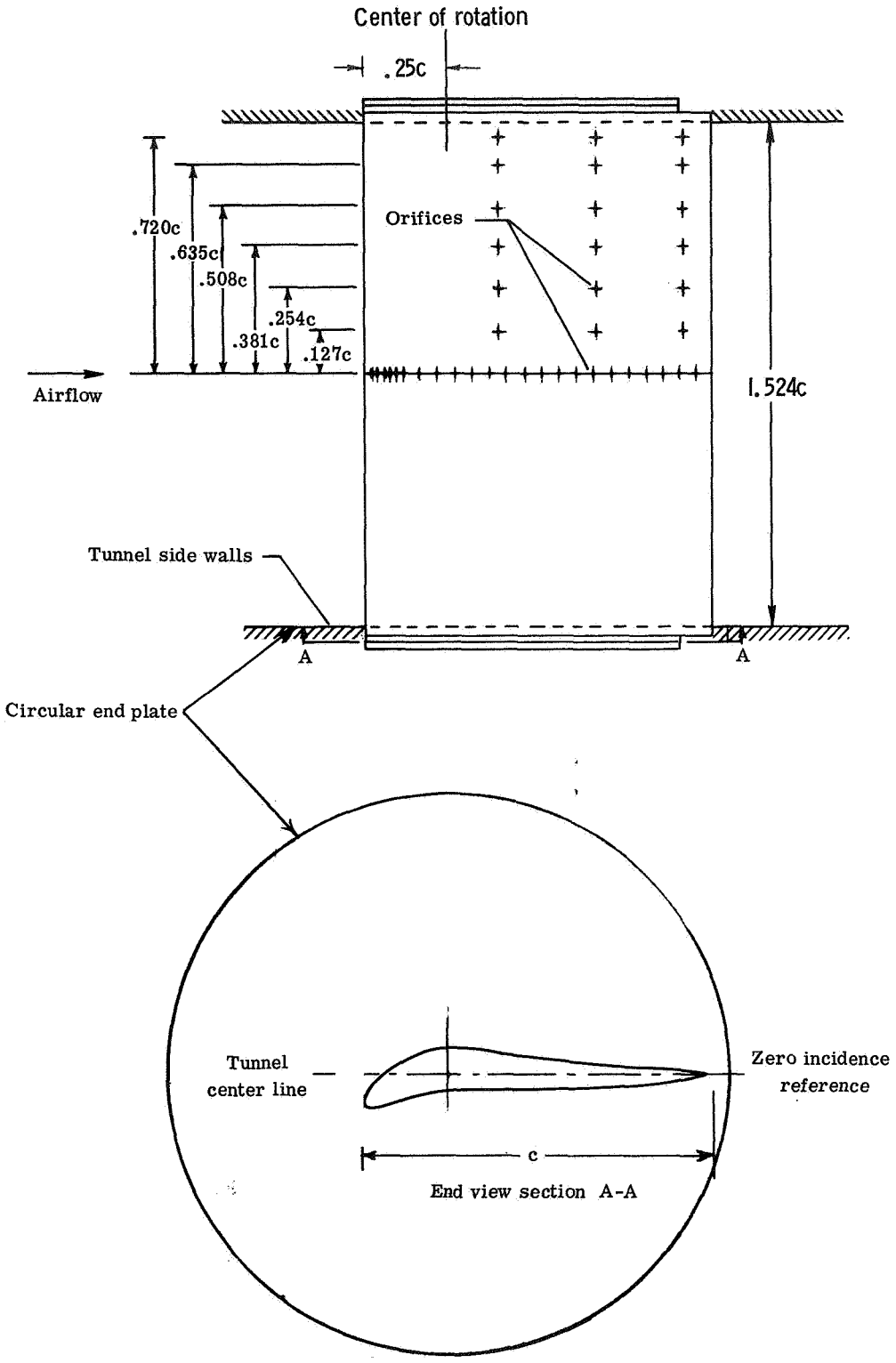

Figure 4.- Airfoil mounted in wind tunnel. All dimensions in terms of airfoil chord c = 60 cm (23.62 in.).

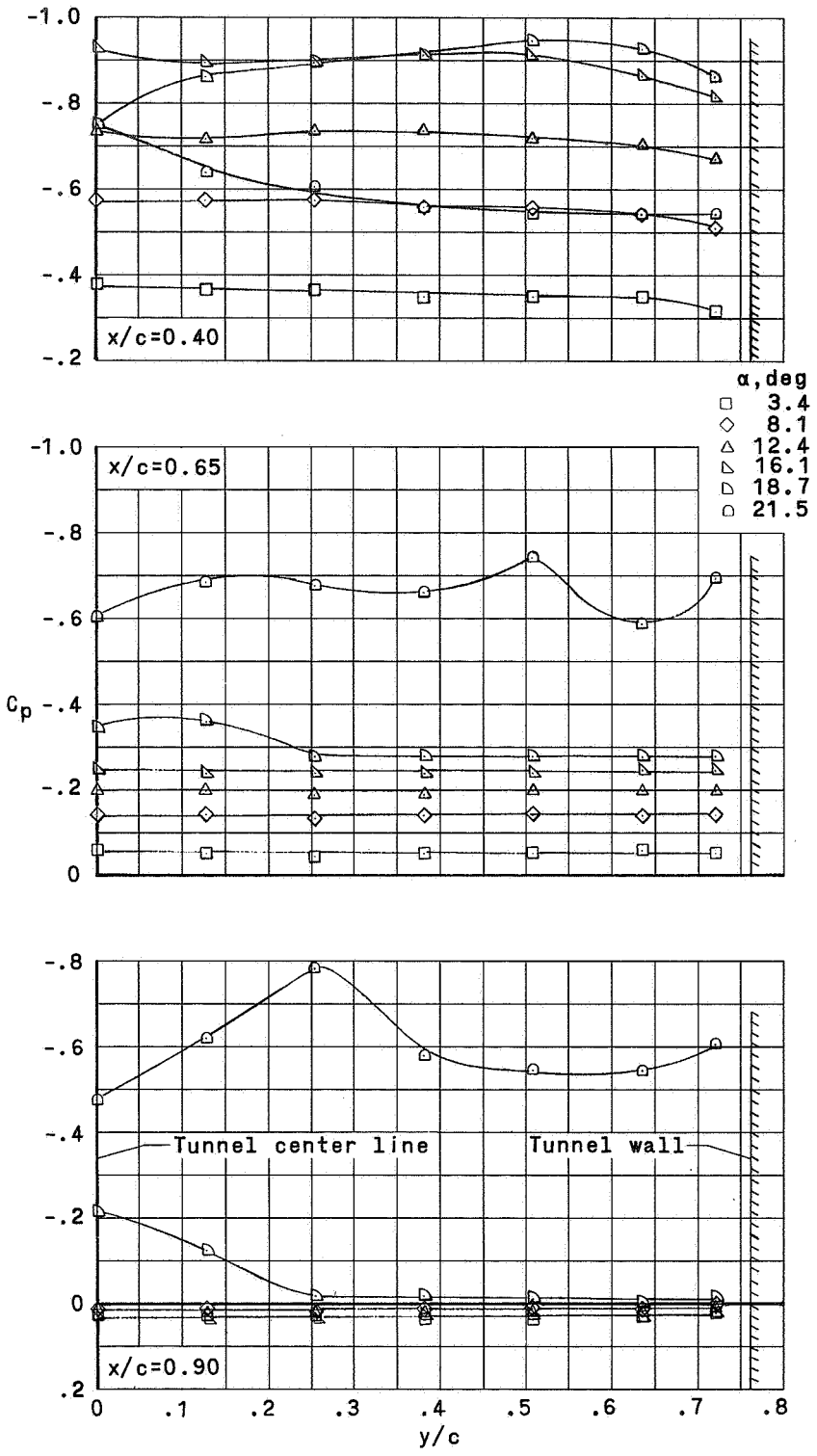

(a) Smooth surface.

Figure 5.- Upper-surface spanwise static pressure distribution. $R \approx 9.2 \times 10^6$; $M = 0.1$.

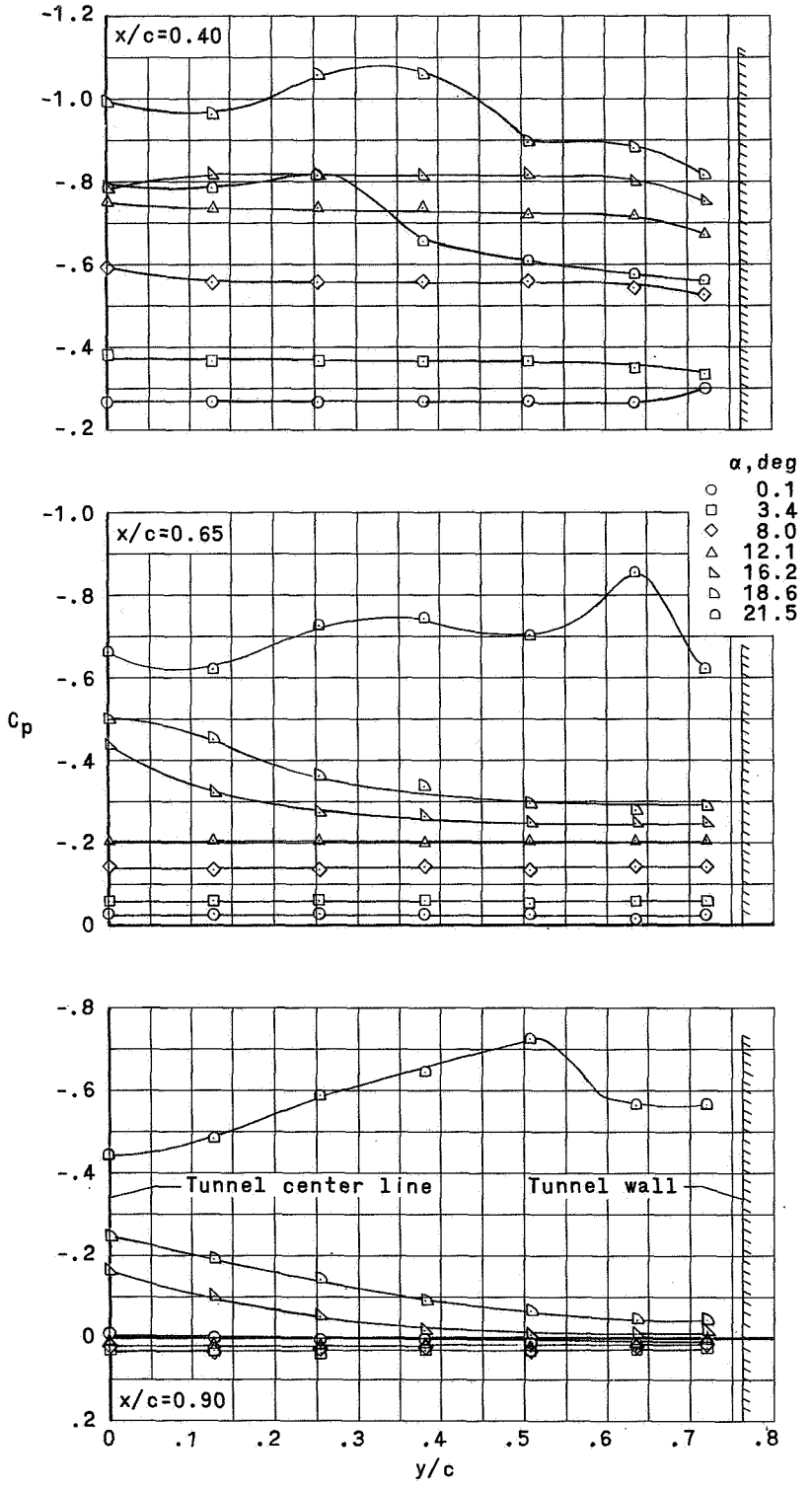

(b) Roughness at 0.25c on upper surface.

Figure 5.- Continued.

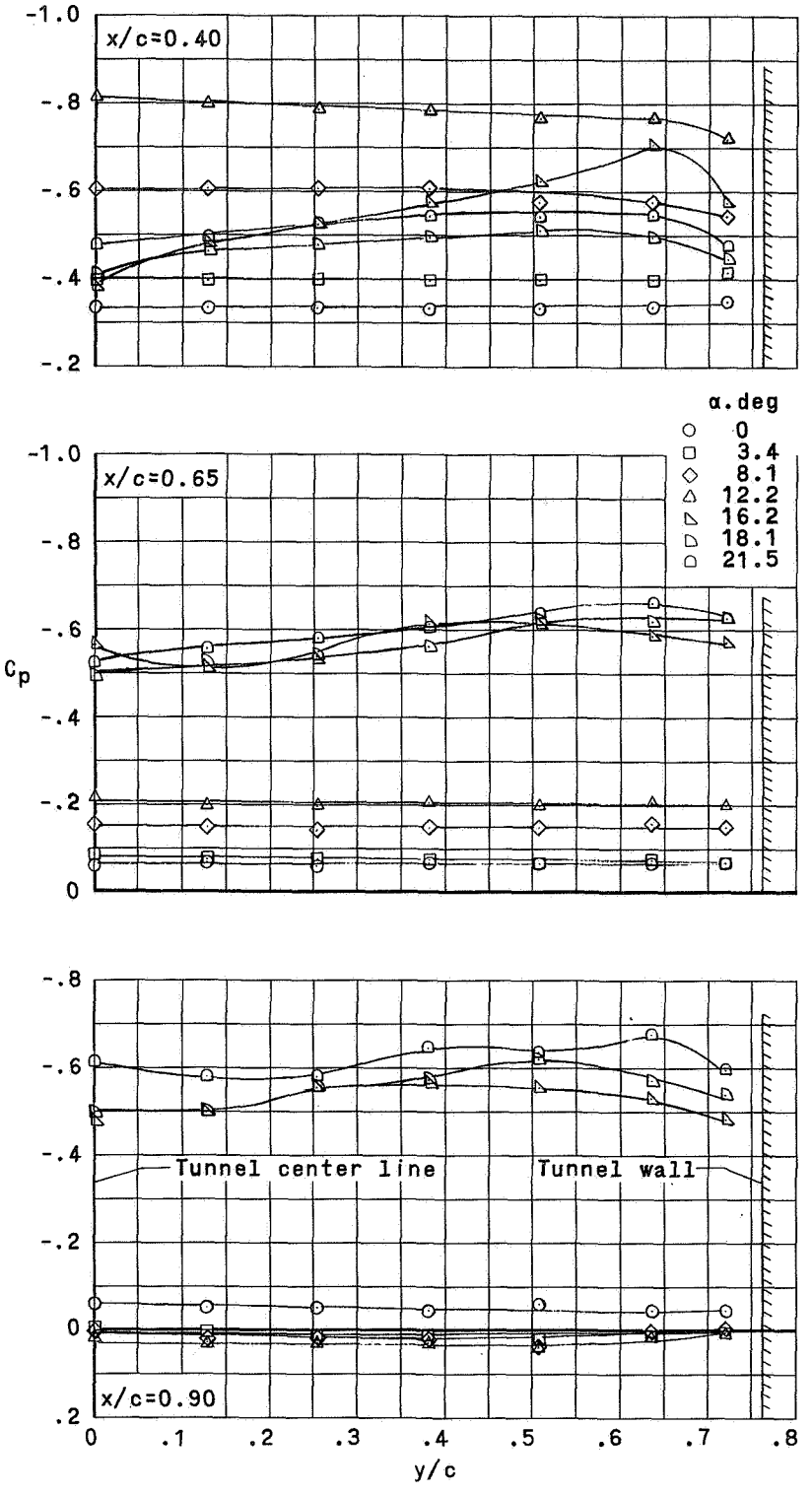

(c) Roughness at leading edge.

Figure 5.- Concluded.

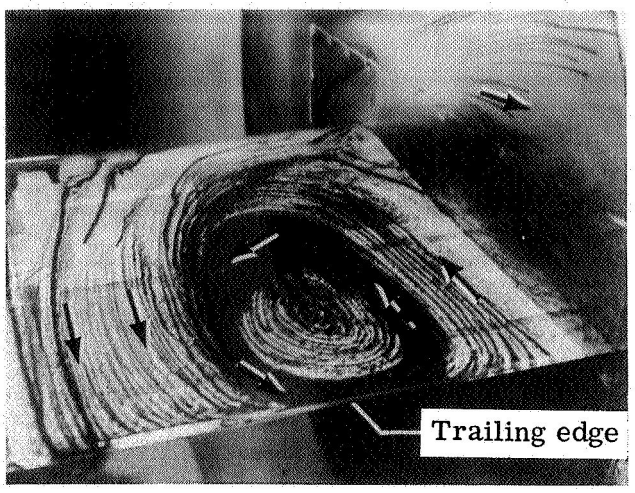

Right-hand side

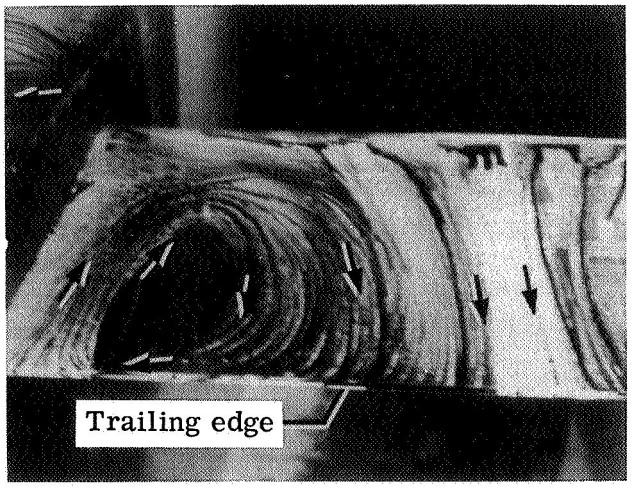

Left-hand side

L-72-6555

Figure 6.- Oil-flow patterns. $\alpha = 18.4^{o}$; $R = 2.0 \times 10^{6}$; $M = 0.1$.

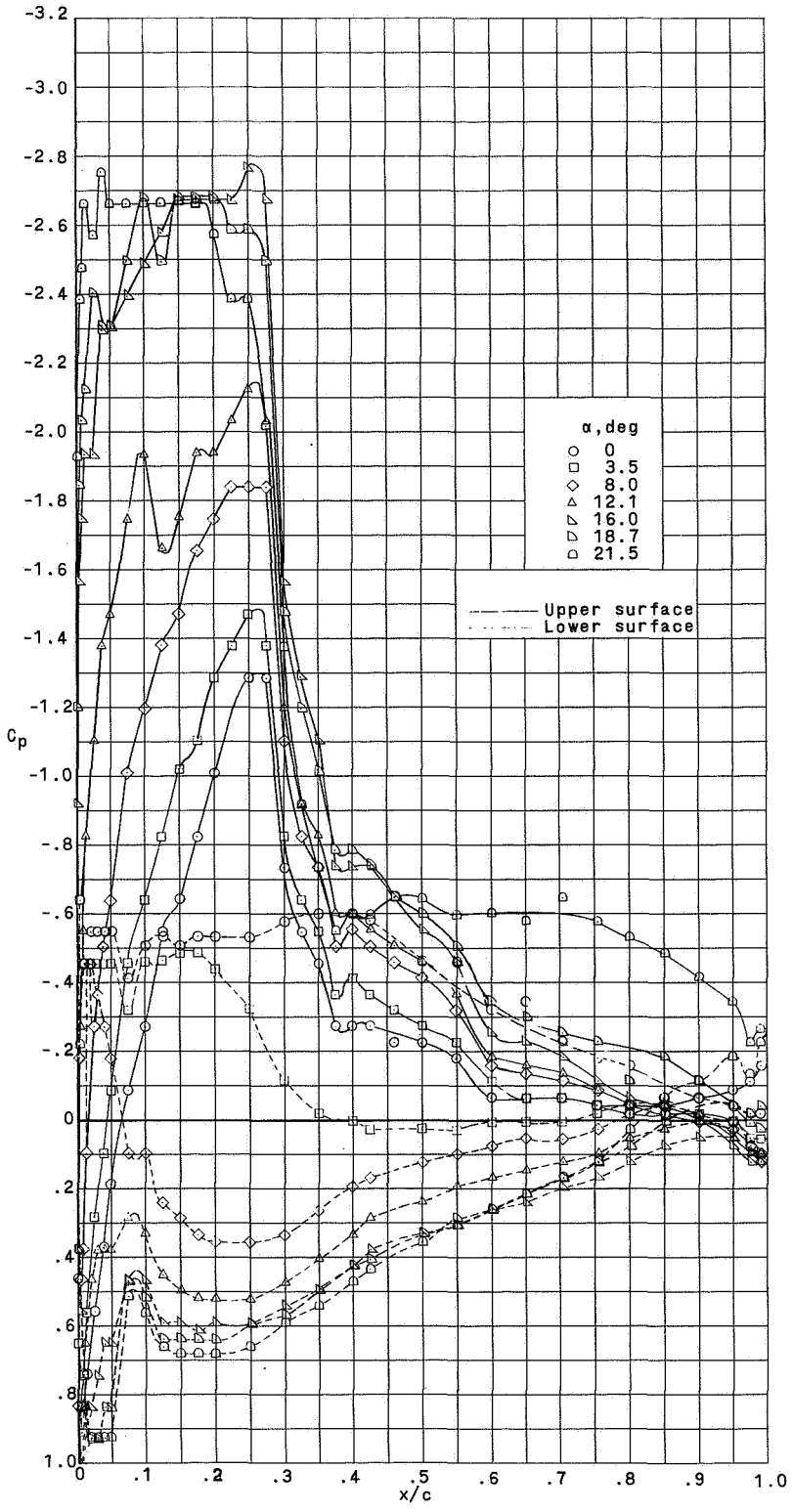

(a) $R = 3.0 \times 10^6$.

Figure 7.- Influence of angle of attack and Reynolds number on airfoil pressure distribution with smooth surface. M = 0.1.

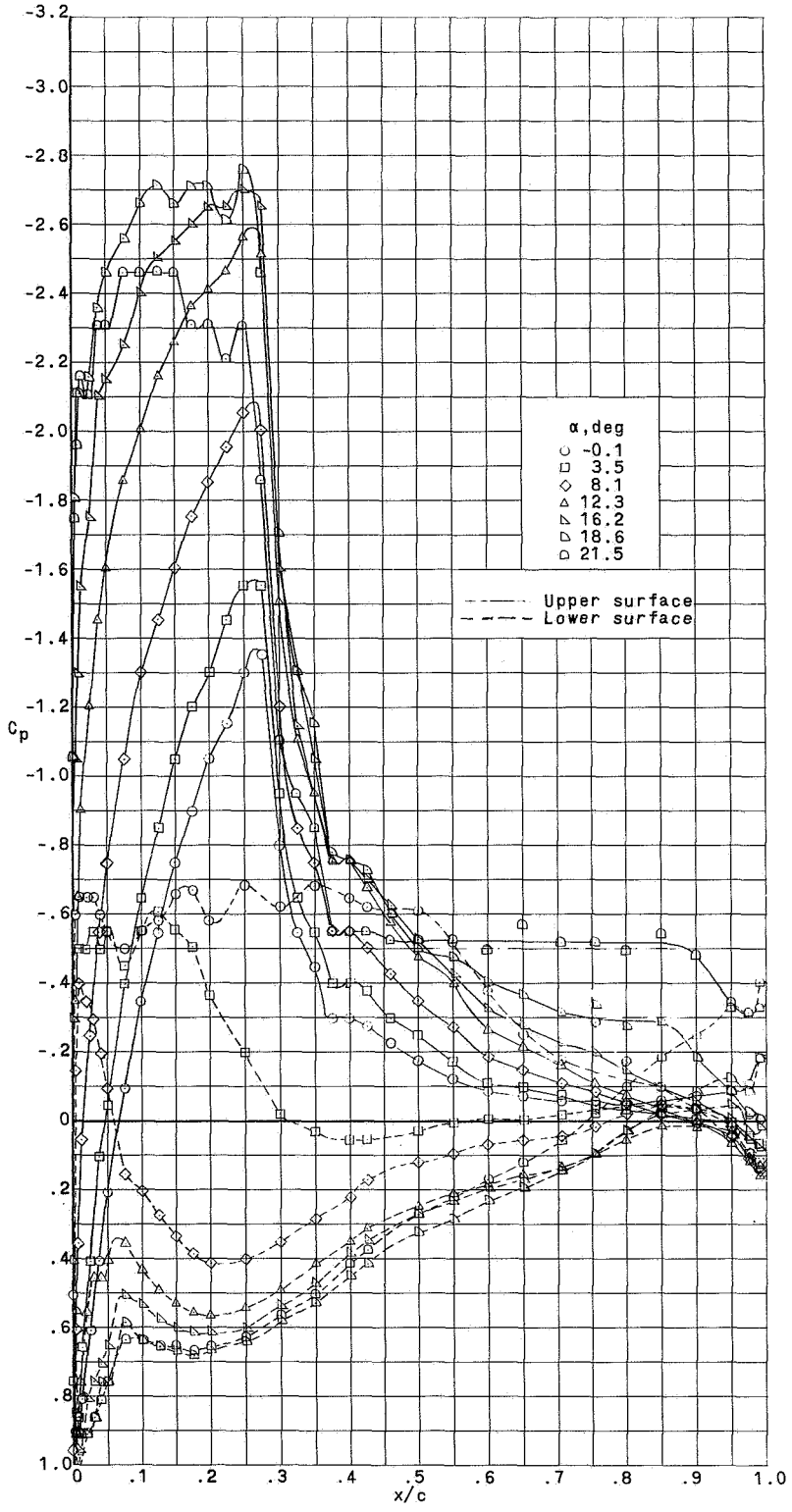

(b) $R = 5.7 \times 10^6$.

Figure 7.- Continued.

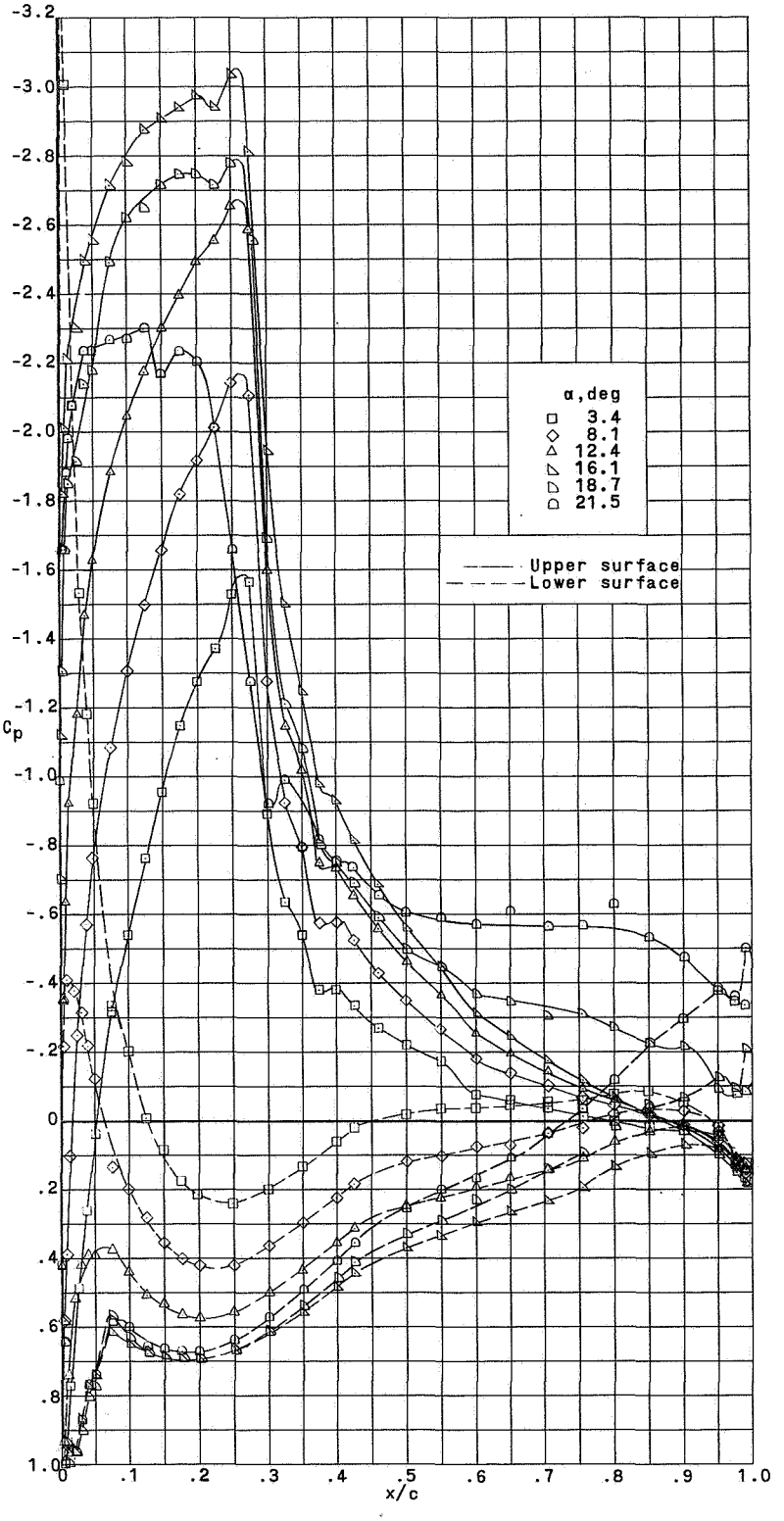

(c) $R = 9.3 \times 10^6$.

Figure 7.- Continued.

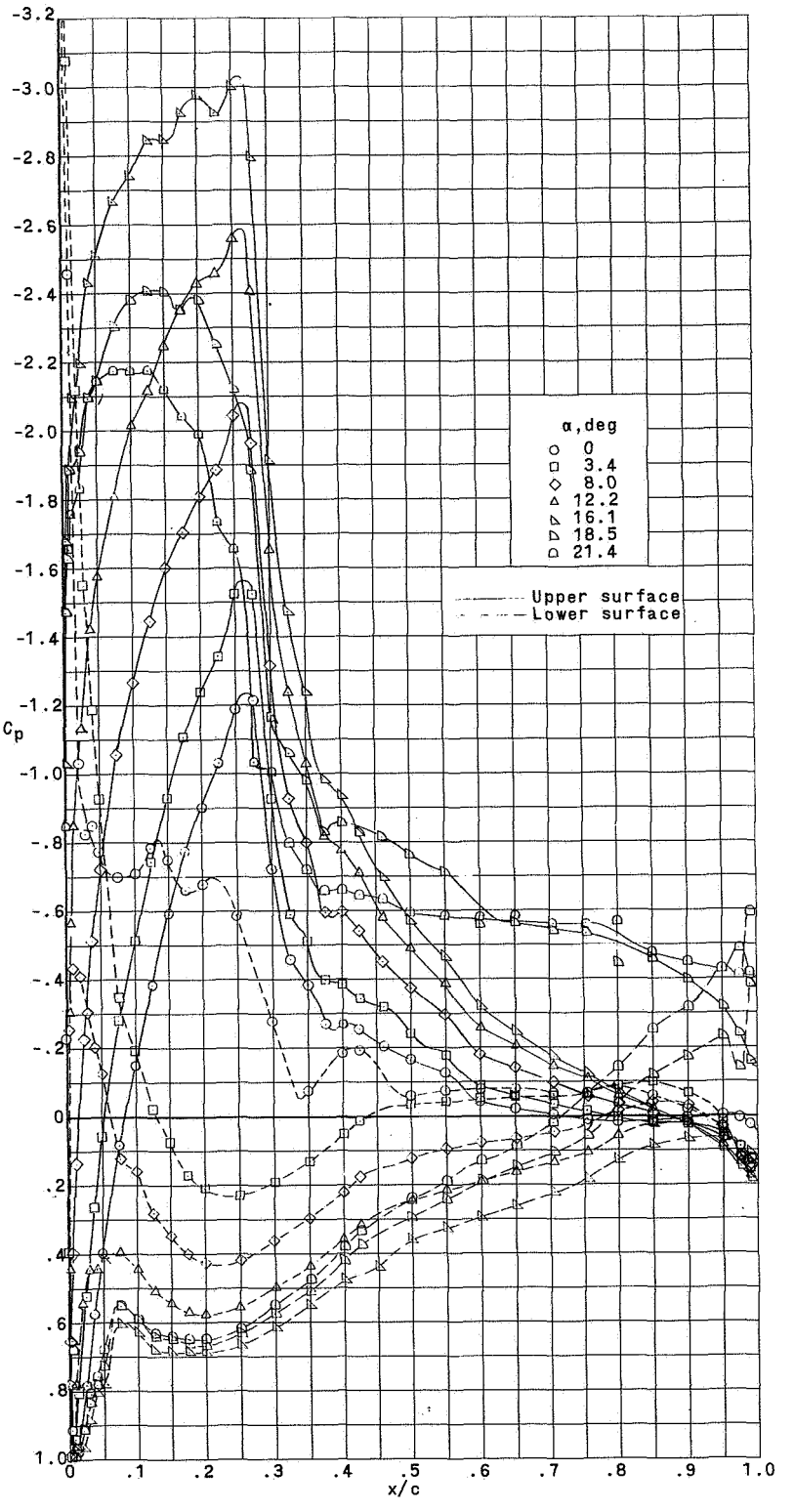

(d) $R = 11.3 \times 10^6$.

Figure 7.- Continued.

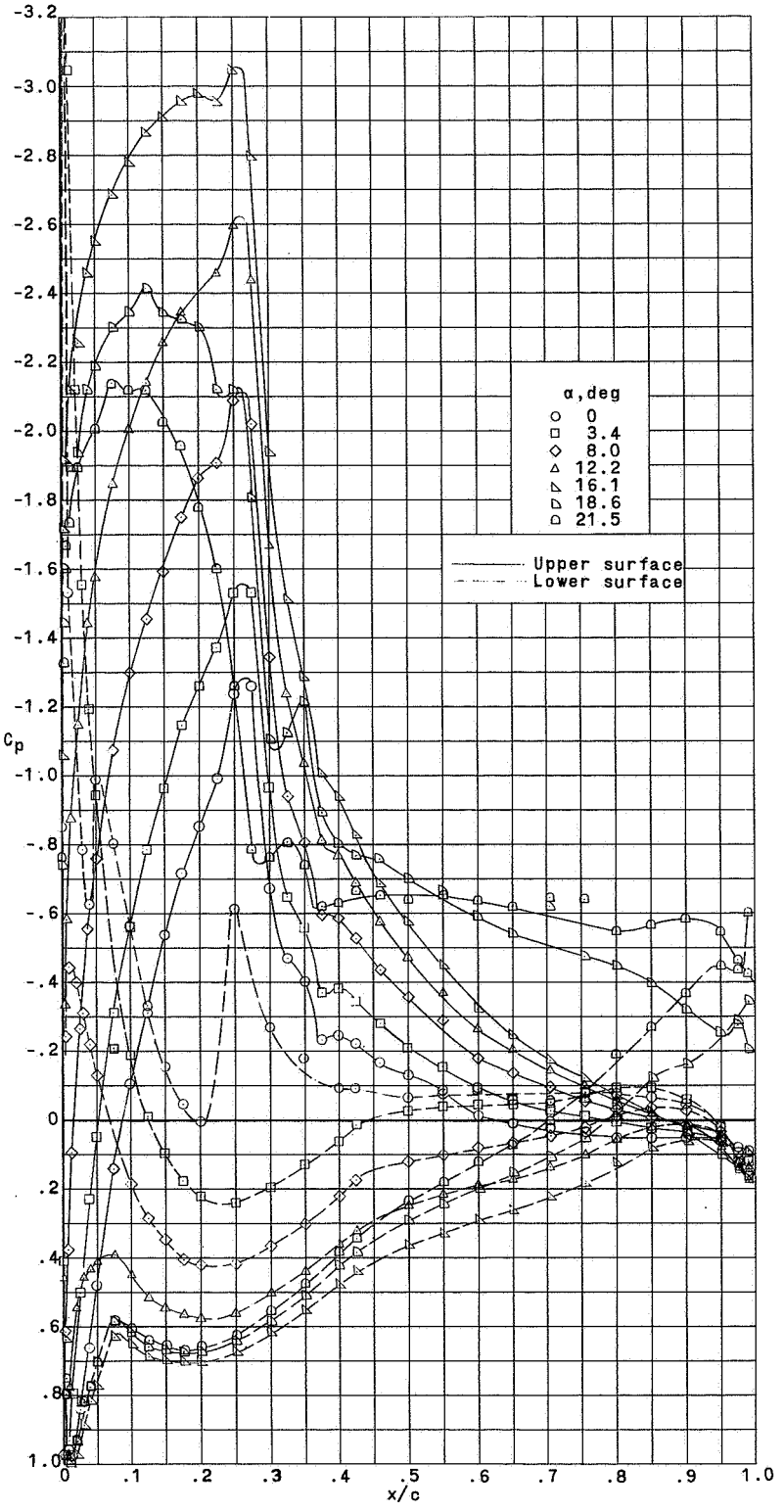

(e) $R = 12.8 \times 10^6$.

Figure 7.- Concluded.

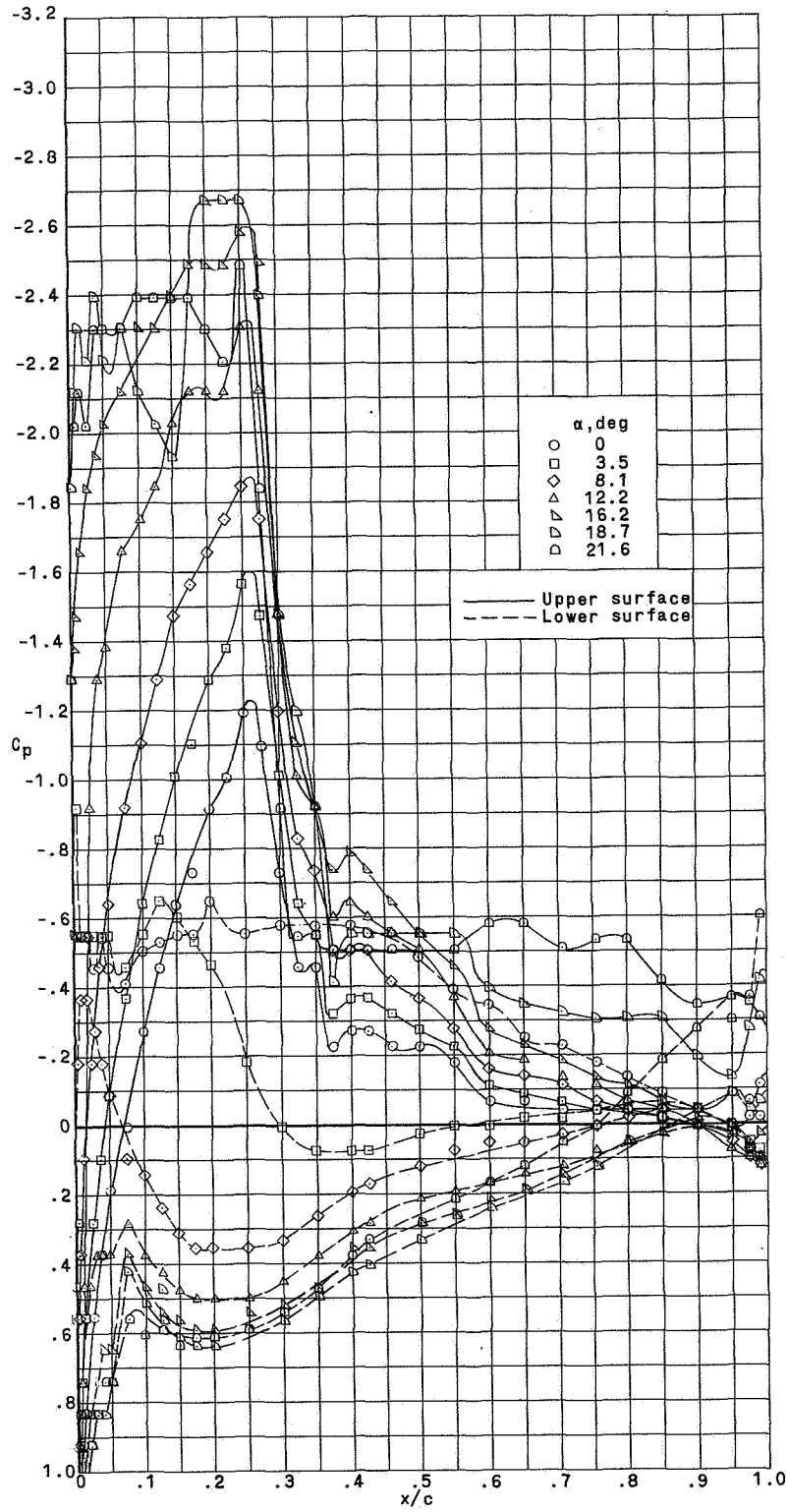

(a) $R = 3.0 \times 10^6$.

Figure 8.- Influence of angle of attack and Reynolds number on airfoil pressure distribution with roughness at 0.25c on upper surface. M = 0.1.

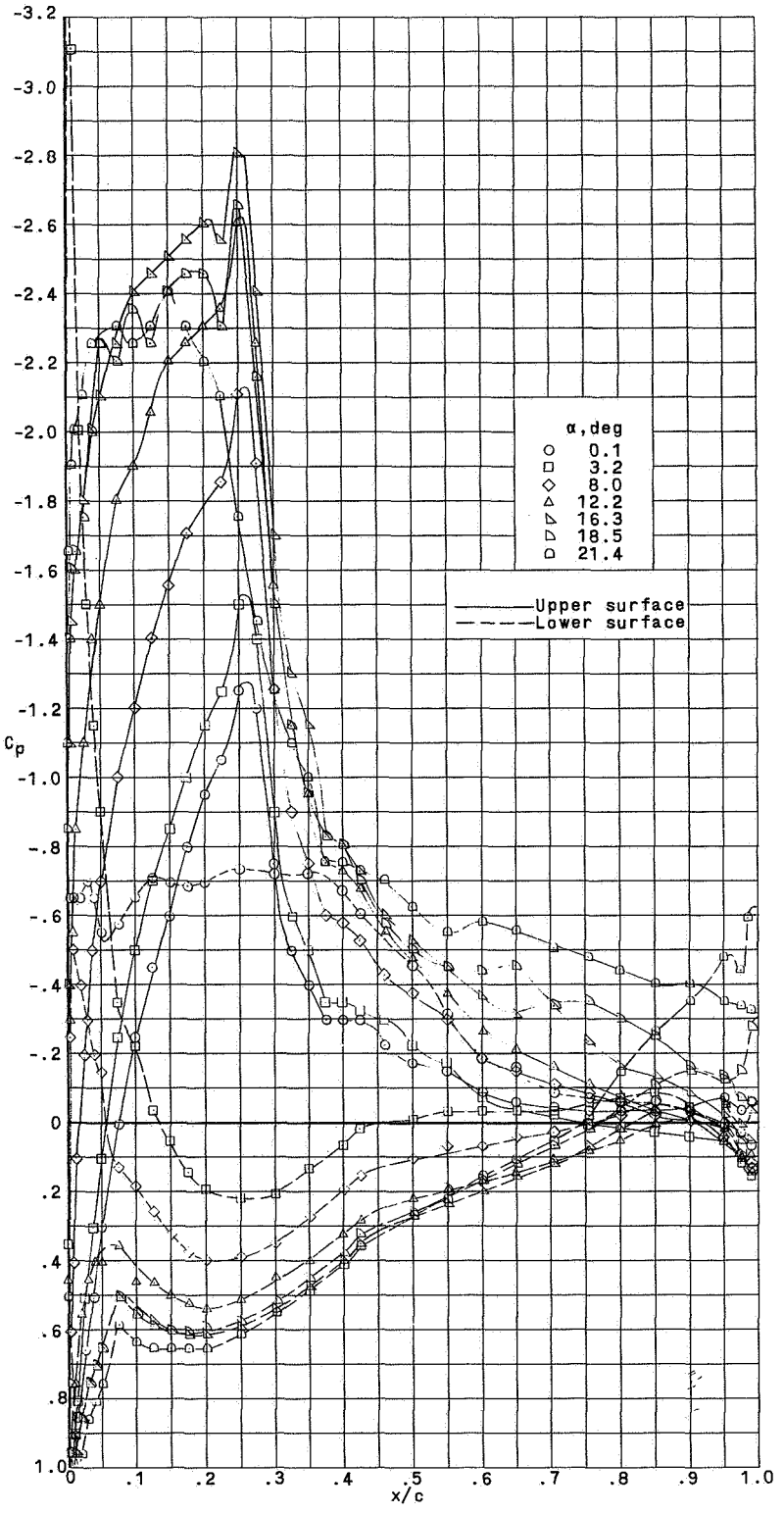

(b) $R = 5.7 \times 10^6$.

Figure 8.- Continued.

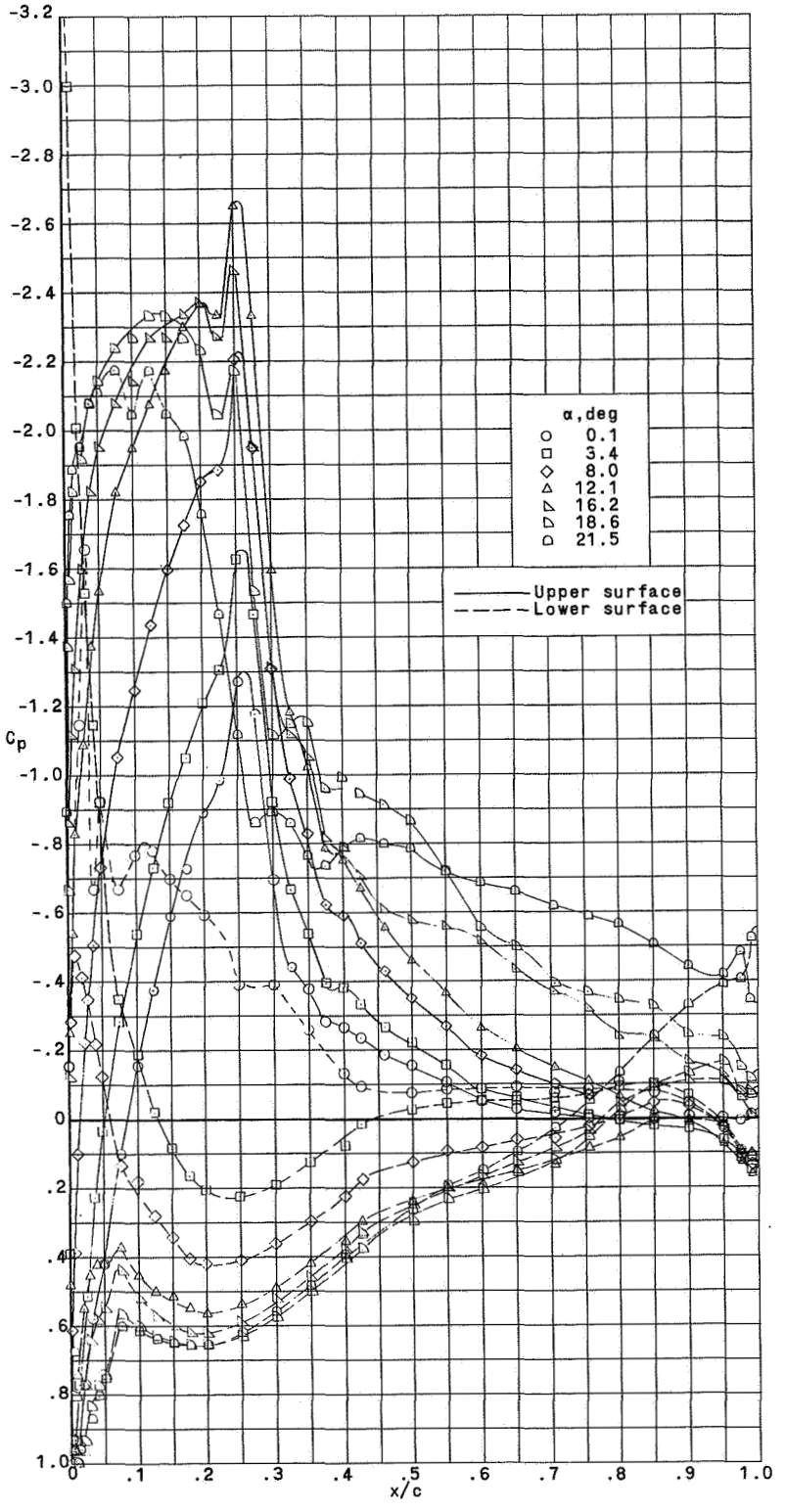

(c) $R = 9.0 \times 10^6$.

Figure 8.- Continued.

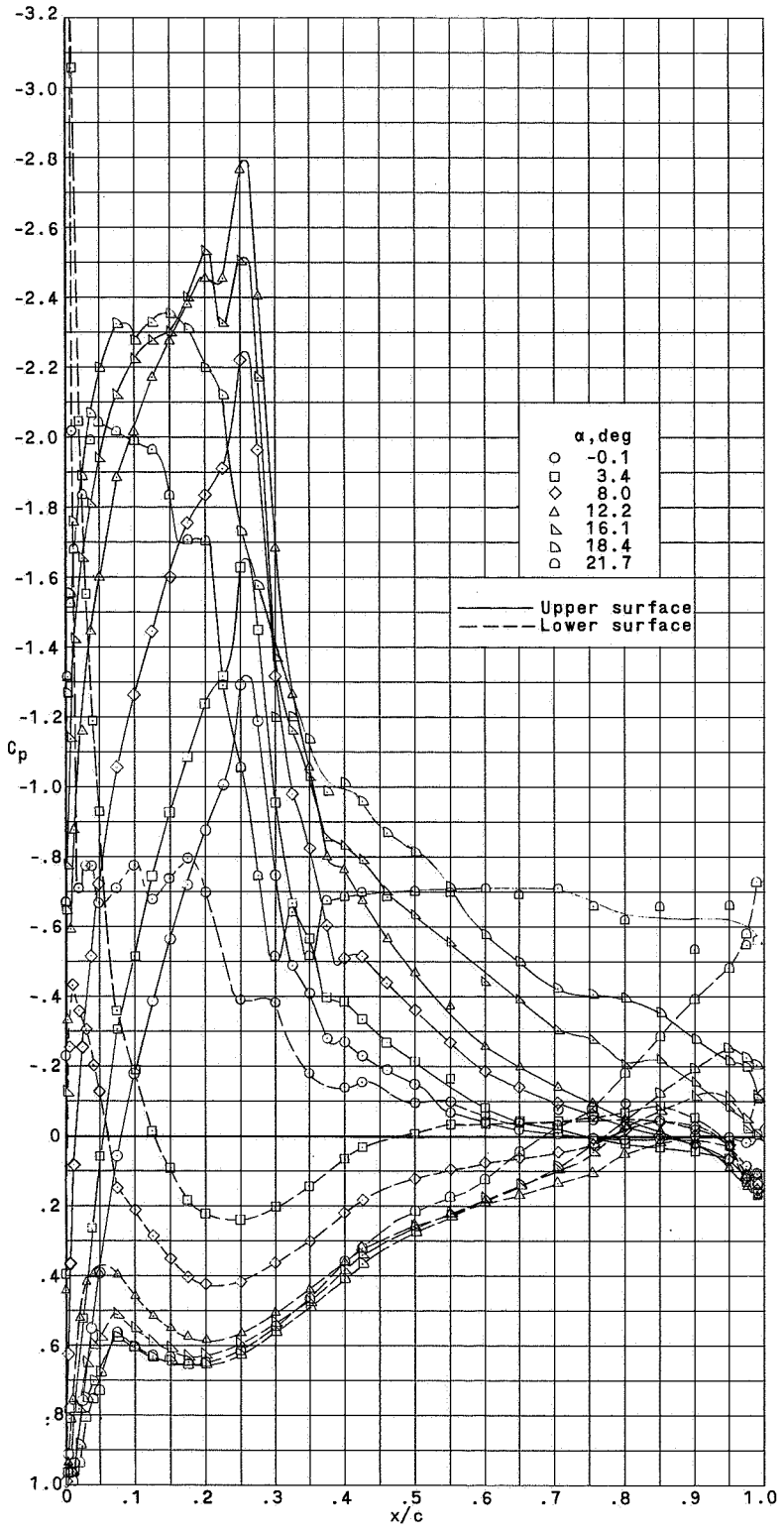

(d) $R = 11.2 \times 10^6$.

Figure 8.- Continued.

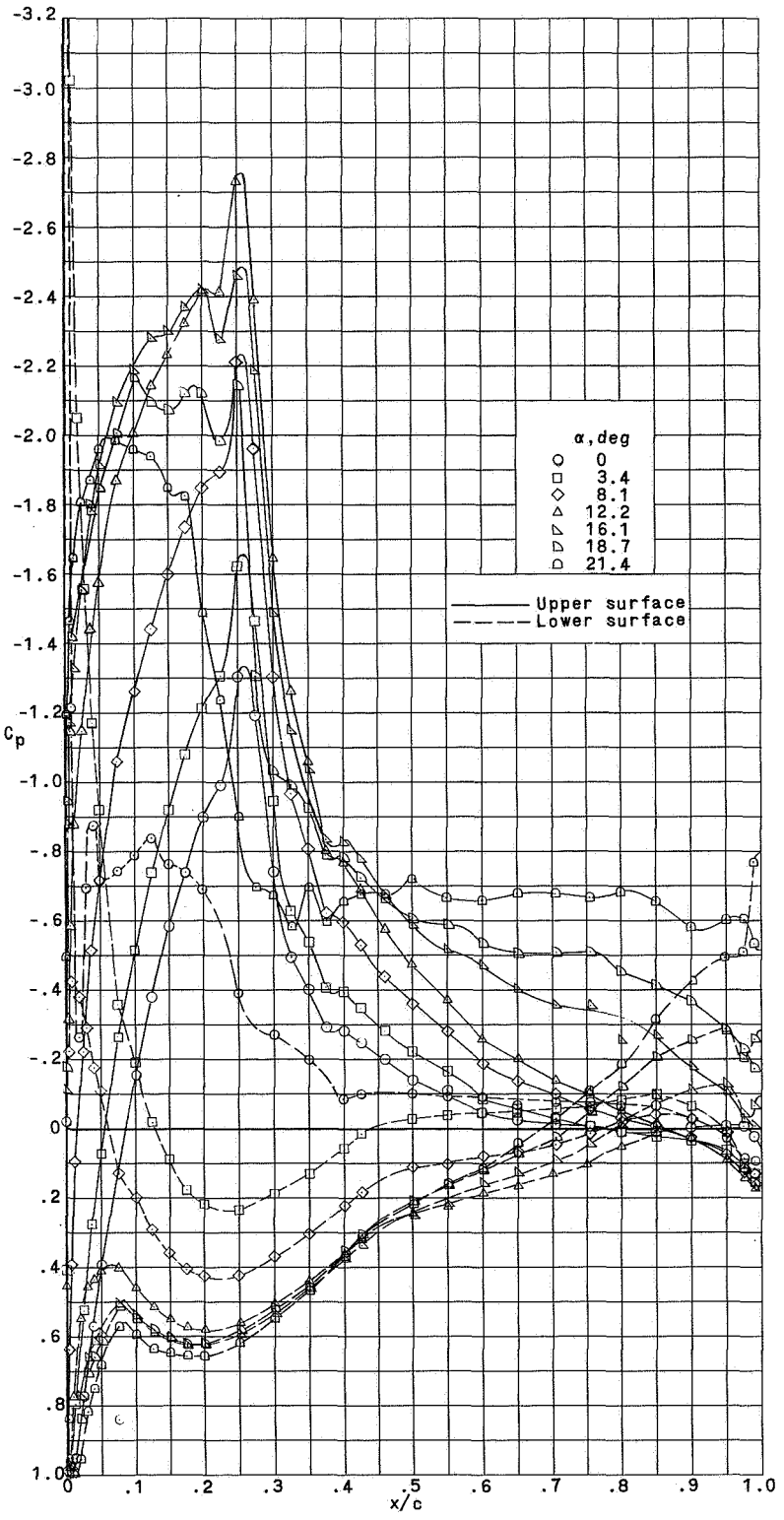

(e) $R = 12.9 \times 10^6$.

Figure 8.- Concluded.

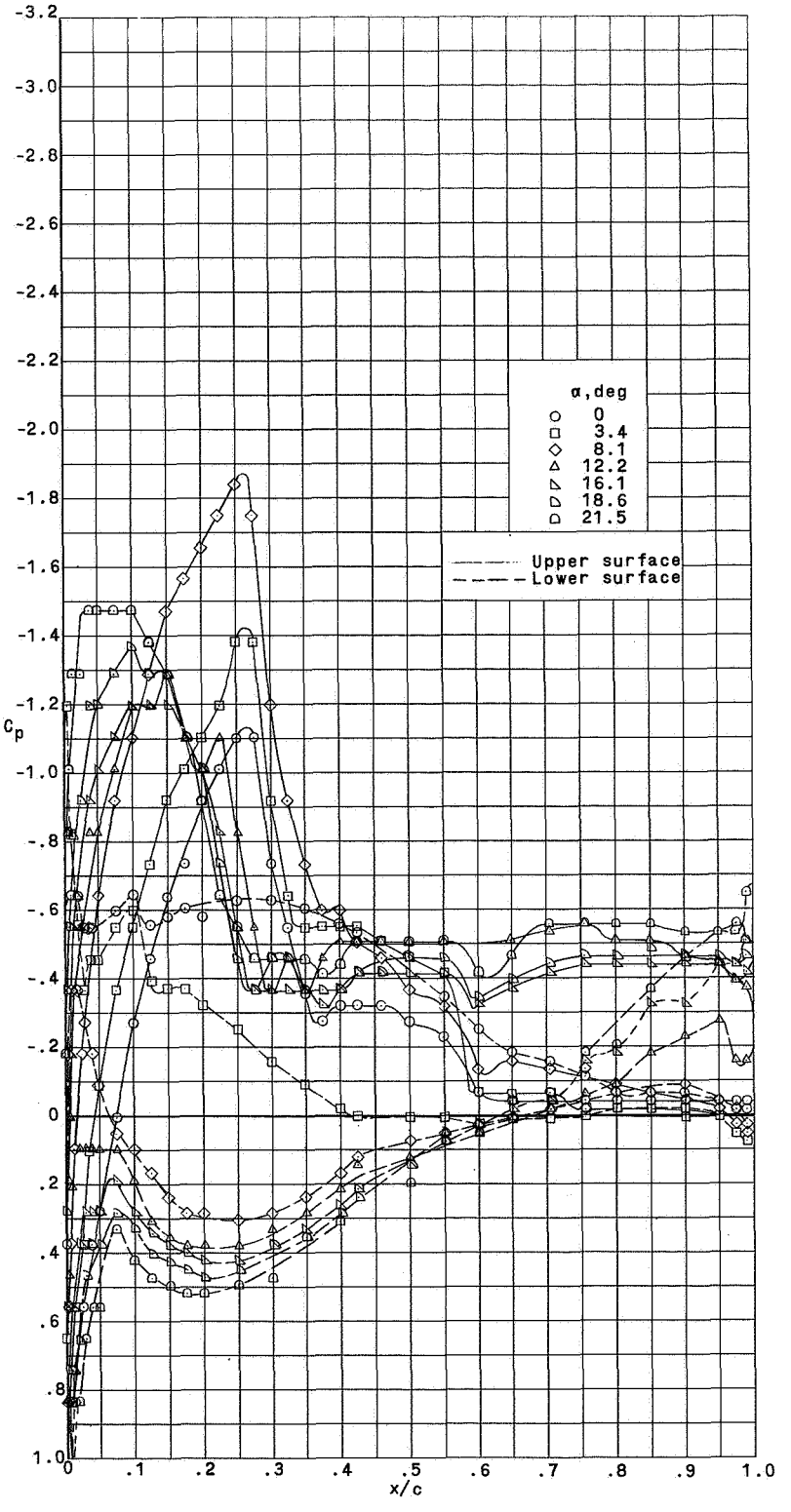

(a) $R = 2.9 \times 10^6$.

Figure 9.- Influence of angle of attack and Reynolds number on airfoil pressure distribution with roughness at leading edge. M = 0.1.

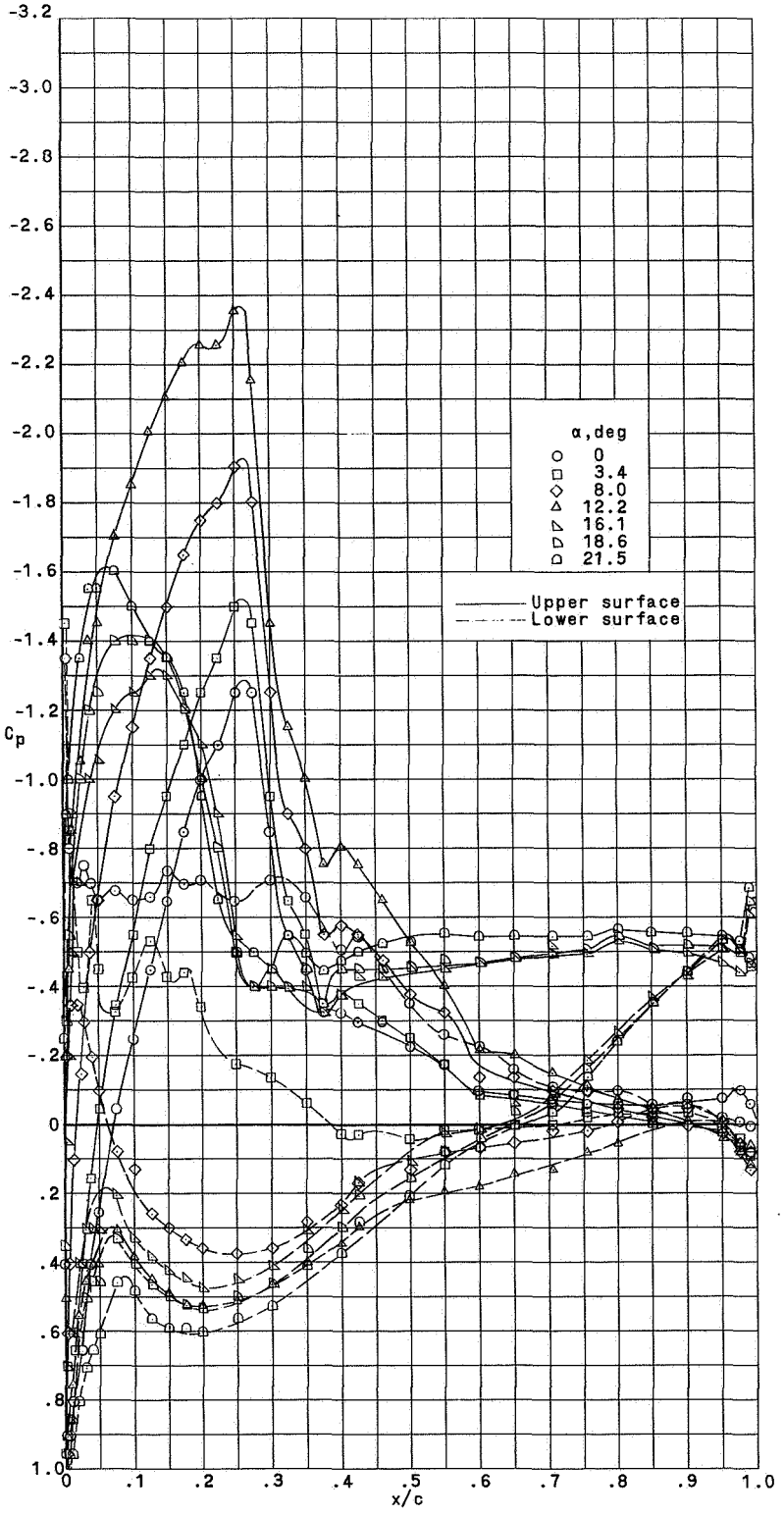

(b) $R = 5.6 \times 10^6$.

Figure 9.- Continued.

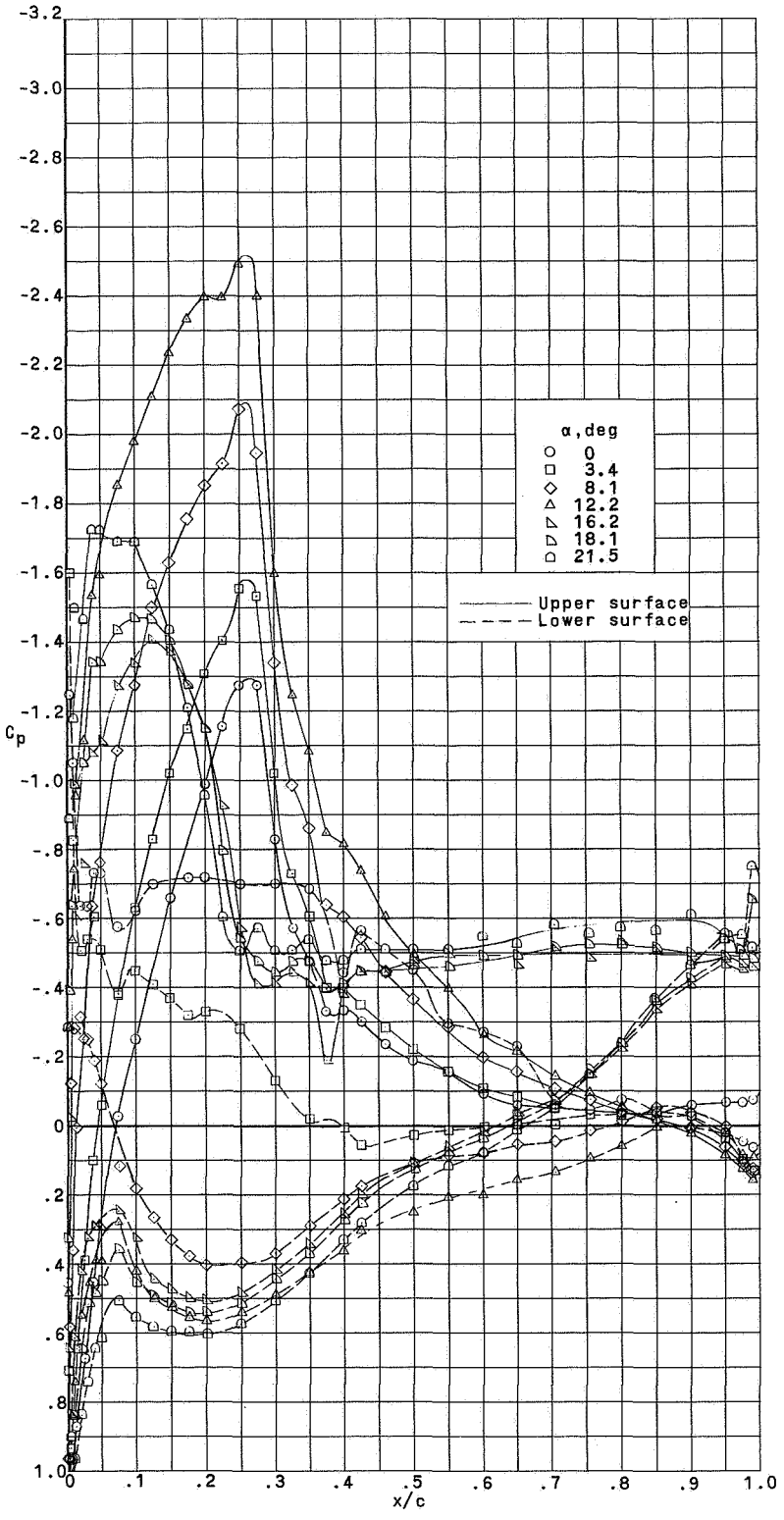

(c) $R = 9.2 \times 10^6$.

Figure 9.- Continued.

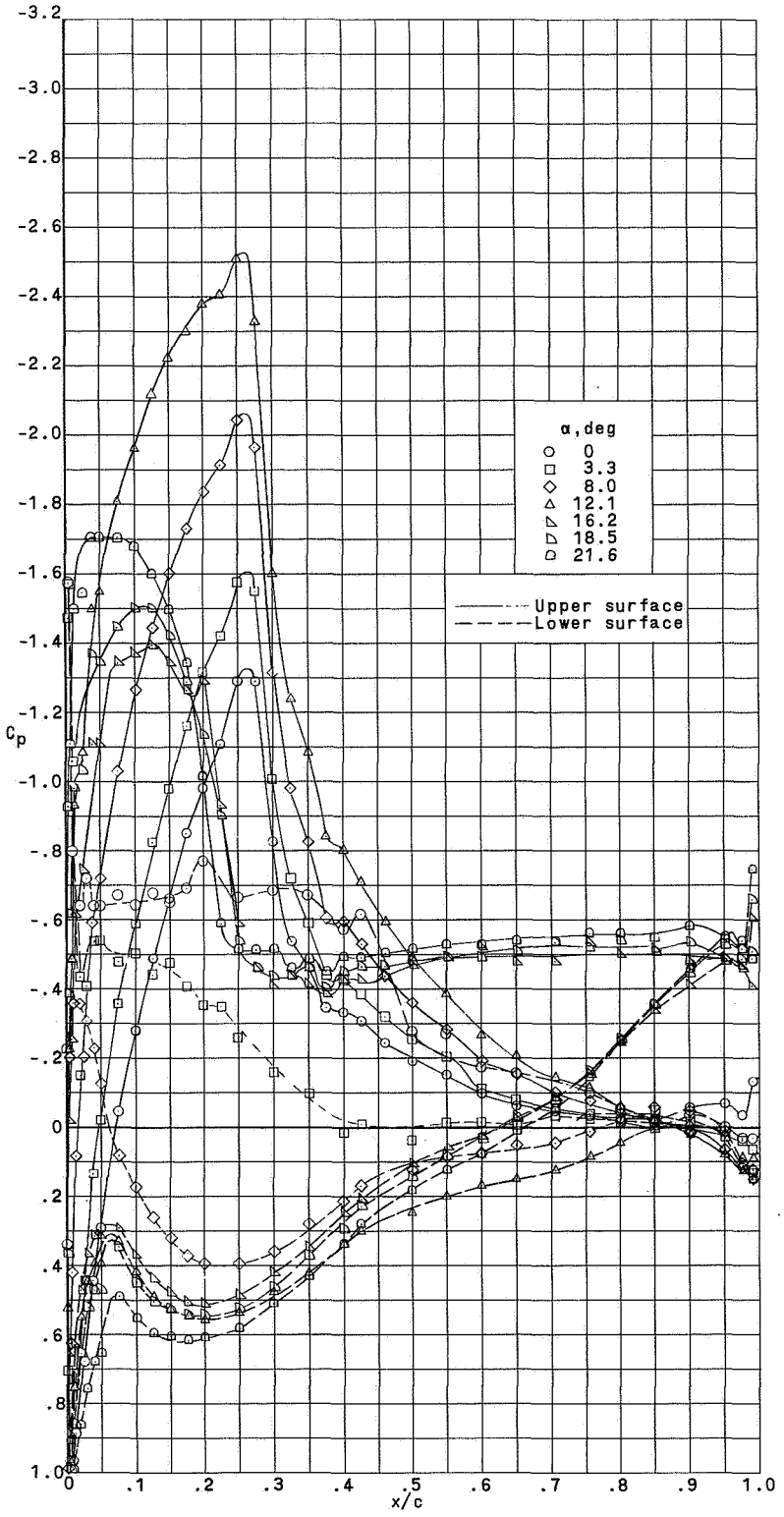

(d) $R = 11.3 \times 10^6$.

Figure 9.- Continued.

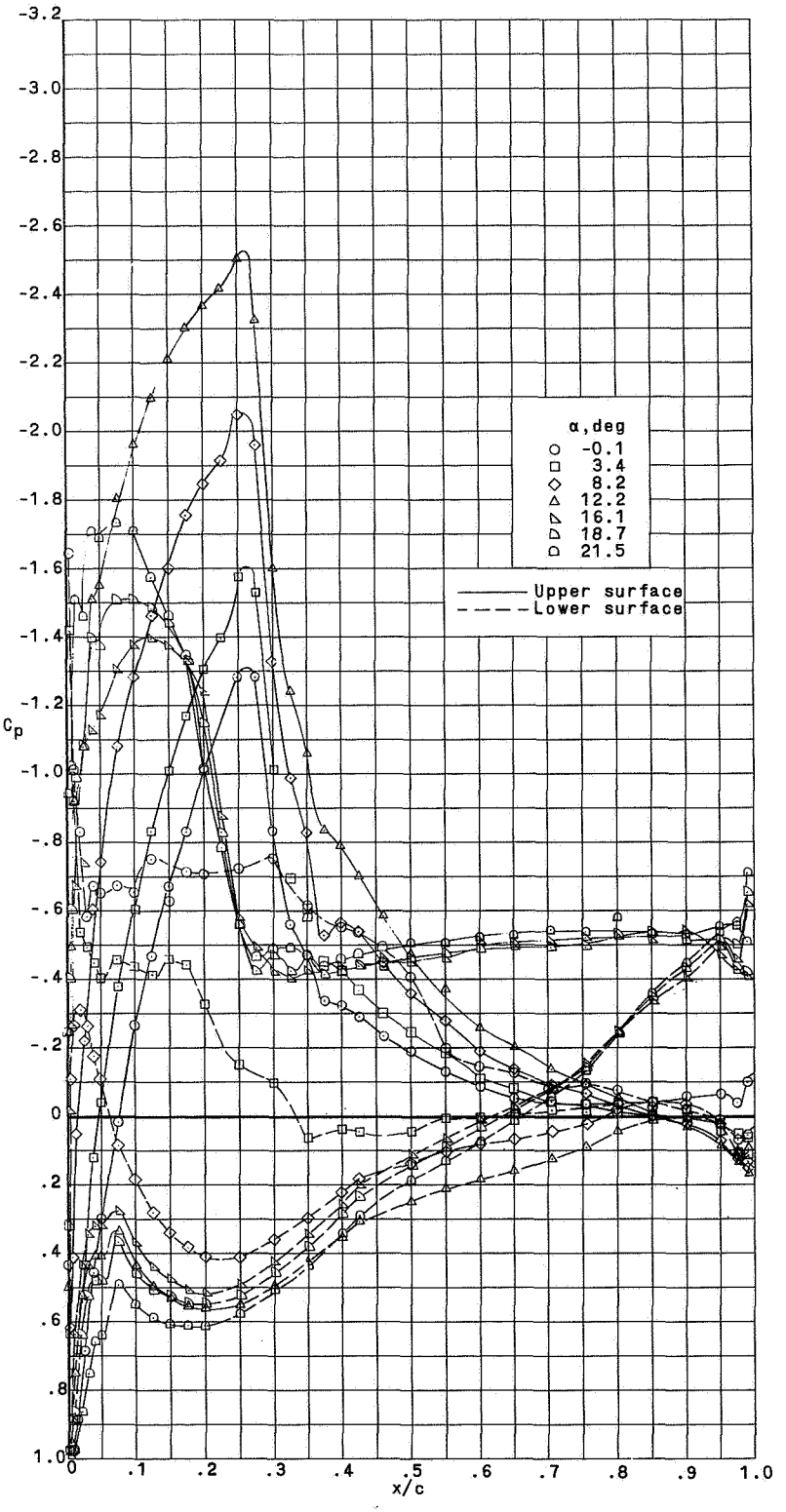

(e) $R = 12.8 \times 10^6$.

Figure 9.- Concluded.

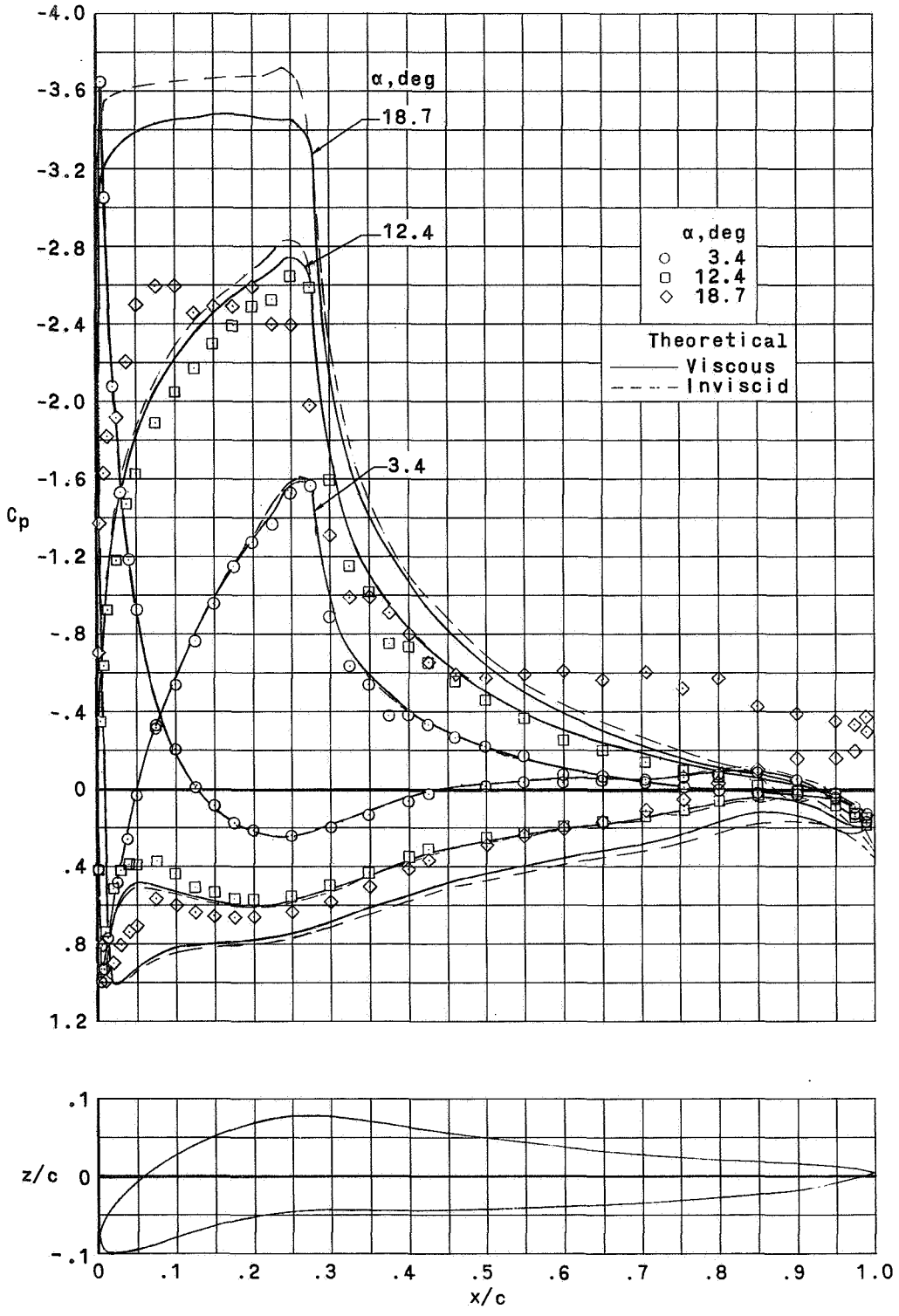

(a) Smooth surface.

Figure 10.- Experimental and theoretical pressure distribution. $R \approx 9.0 \times 10^6$; $M = 0.1$.

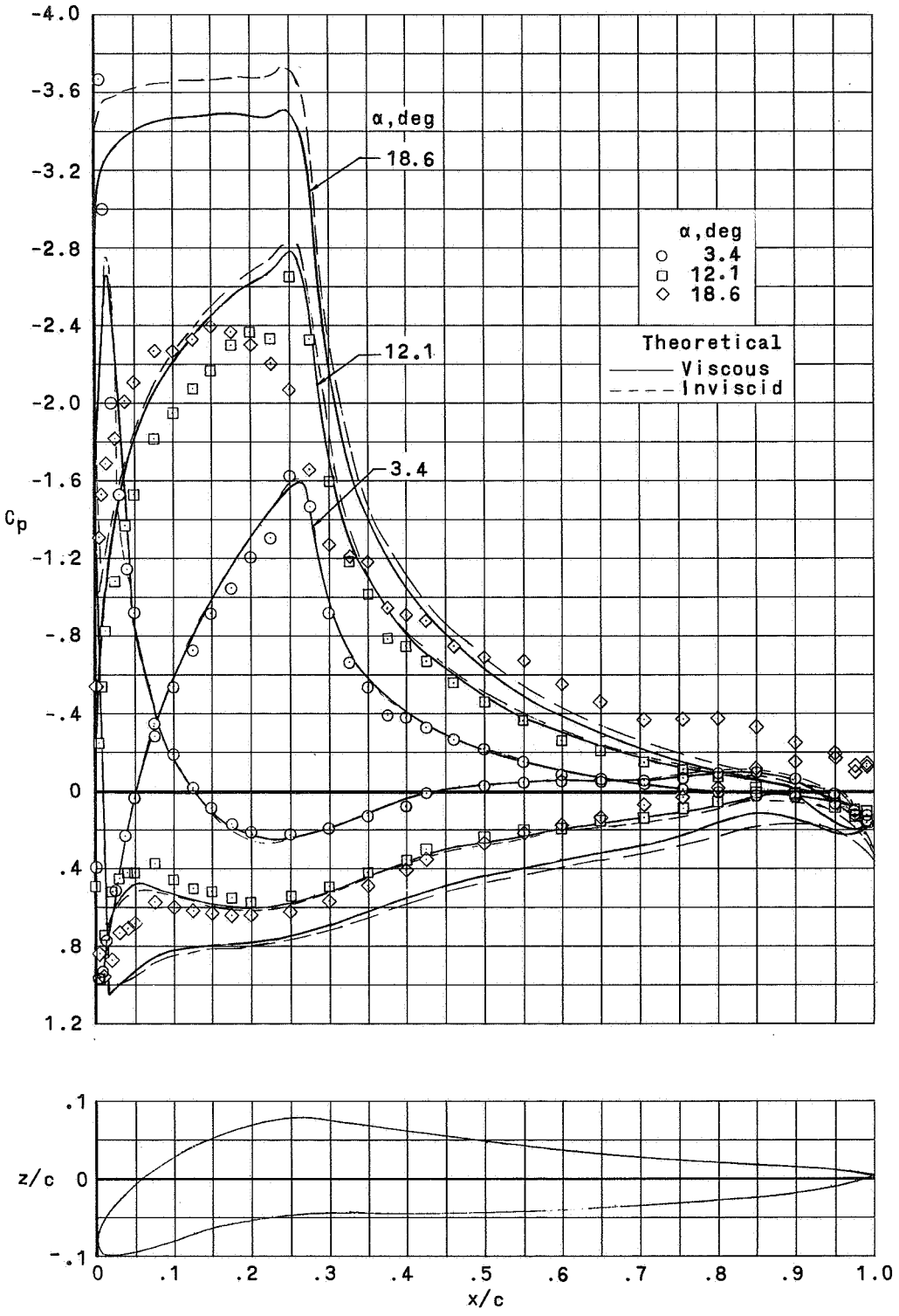

(b) Roughness at 0.25c on upper surface.

Figure 10.- Continued.

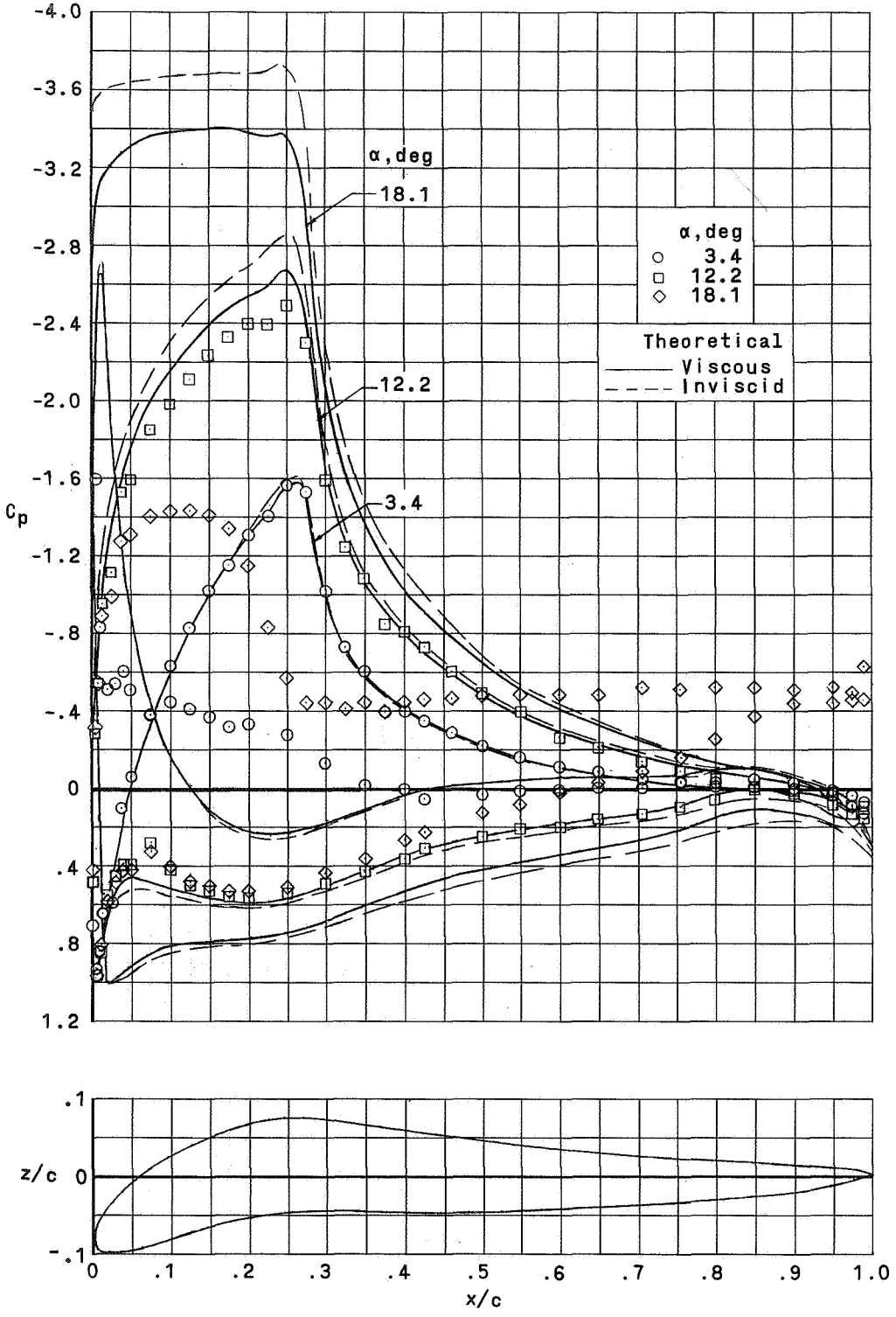

(c) Roughness at leading edge.

Figure 10.- Concluded.

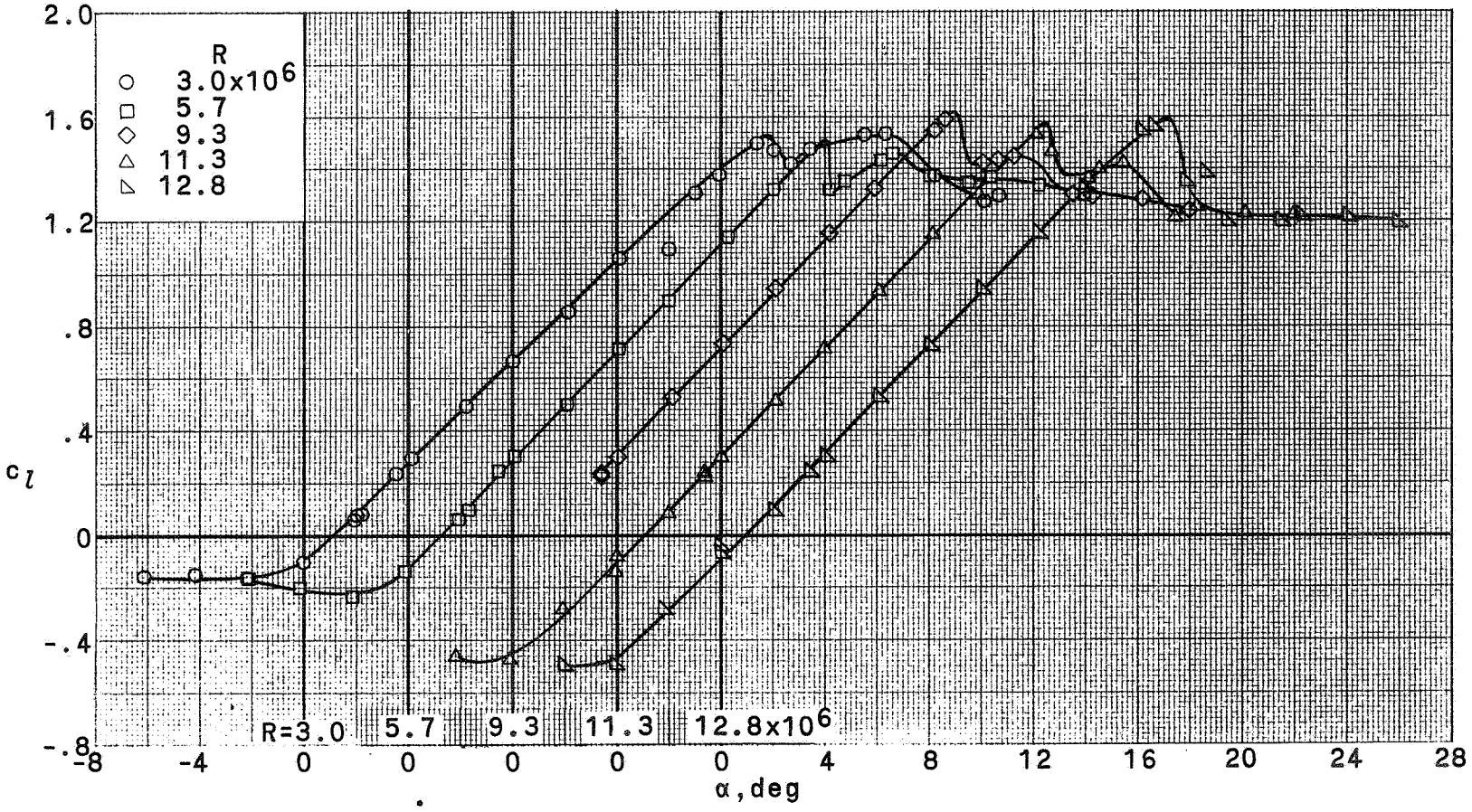

(a) Smooth surface.

Figure 11.- Influence of Reynolds number on section lift coefficient. M = 0.1.

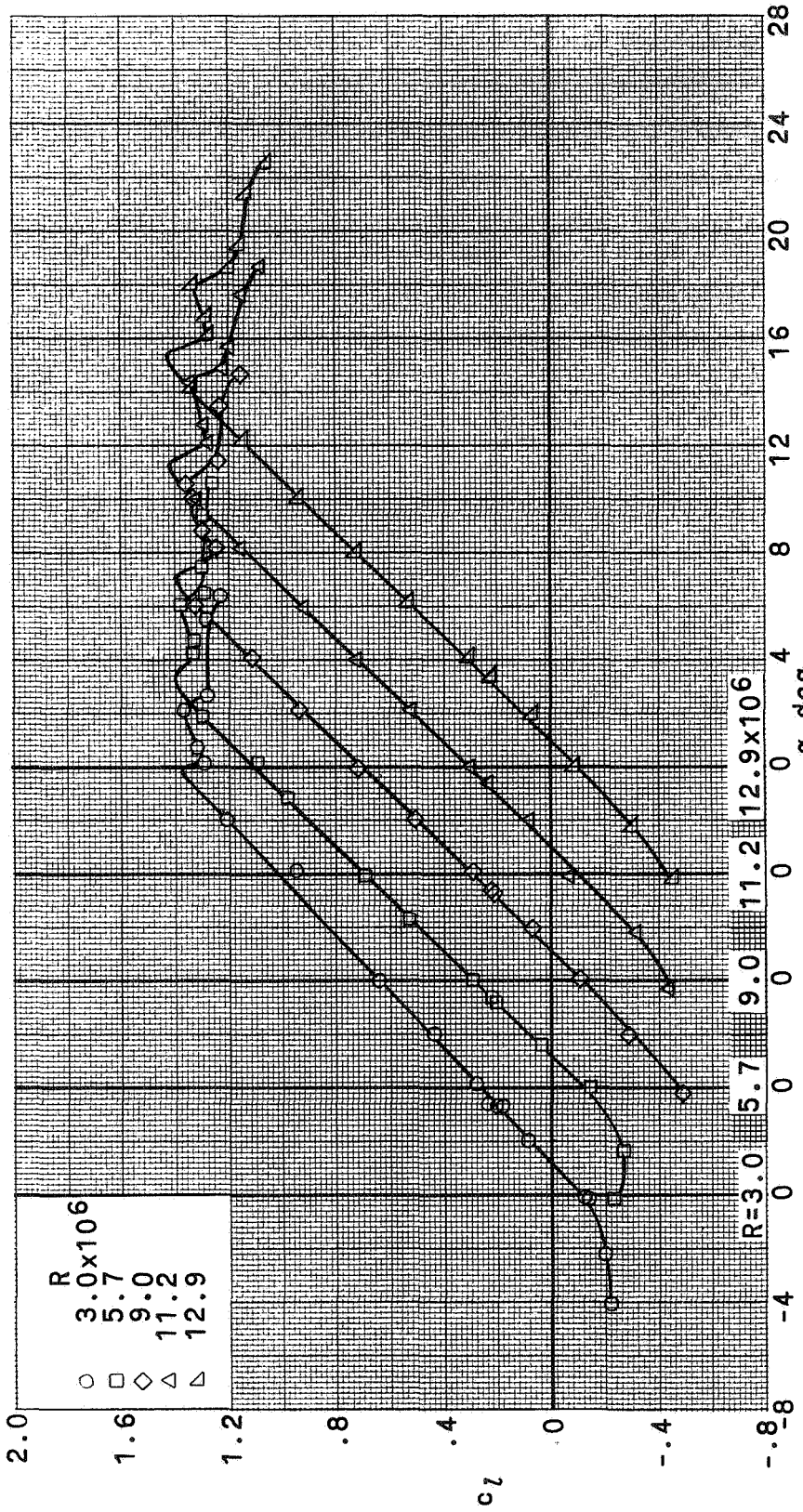

(b) Roughness at 0.25c on upper surface.

Figure 11.- Continued.

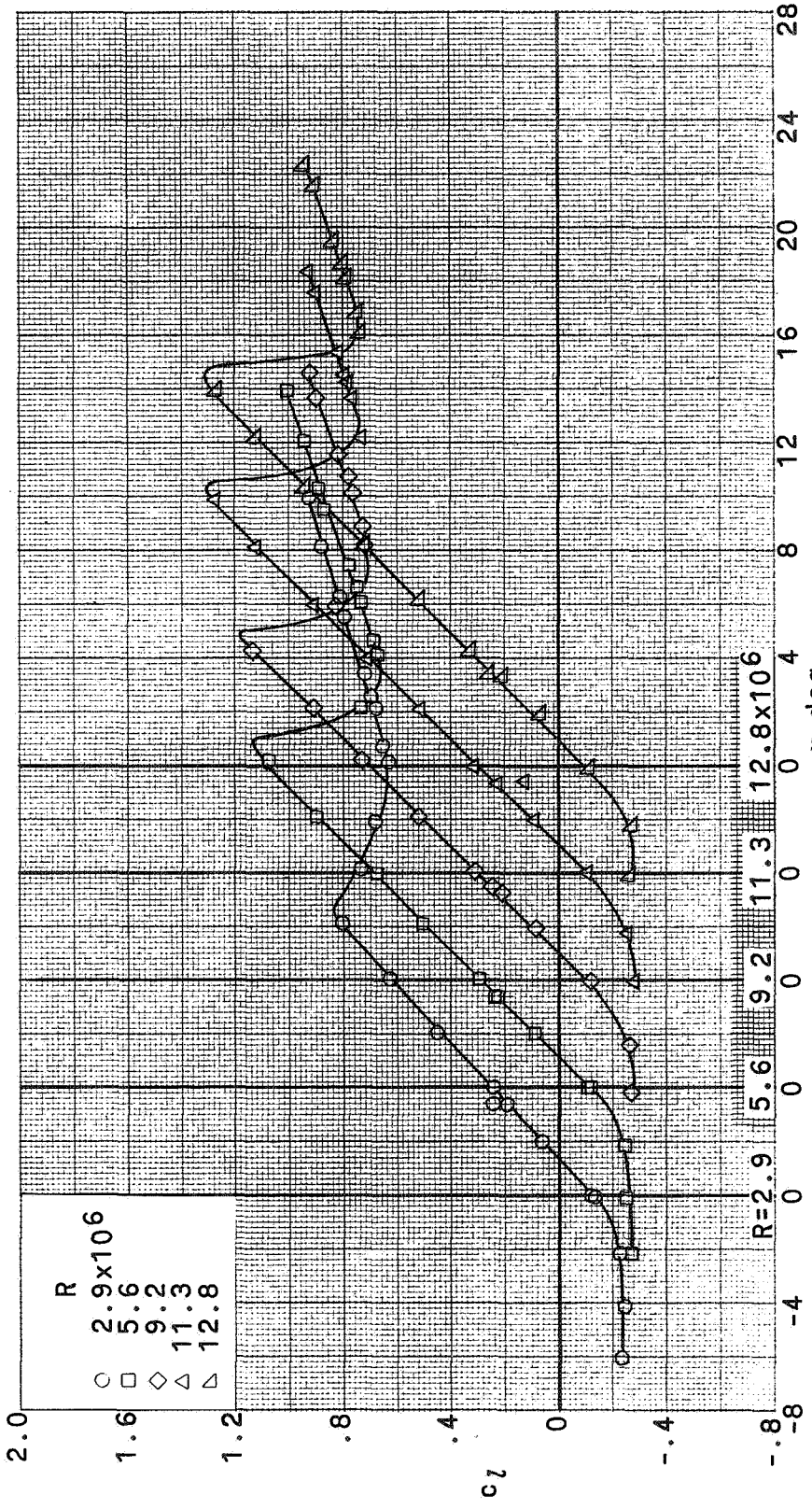

(c) Roughness at leading edge.

Figure 11.- Concluded.

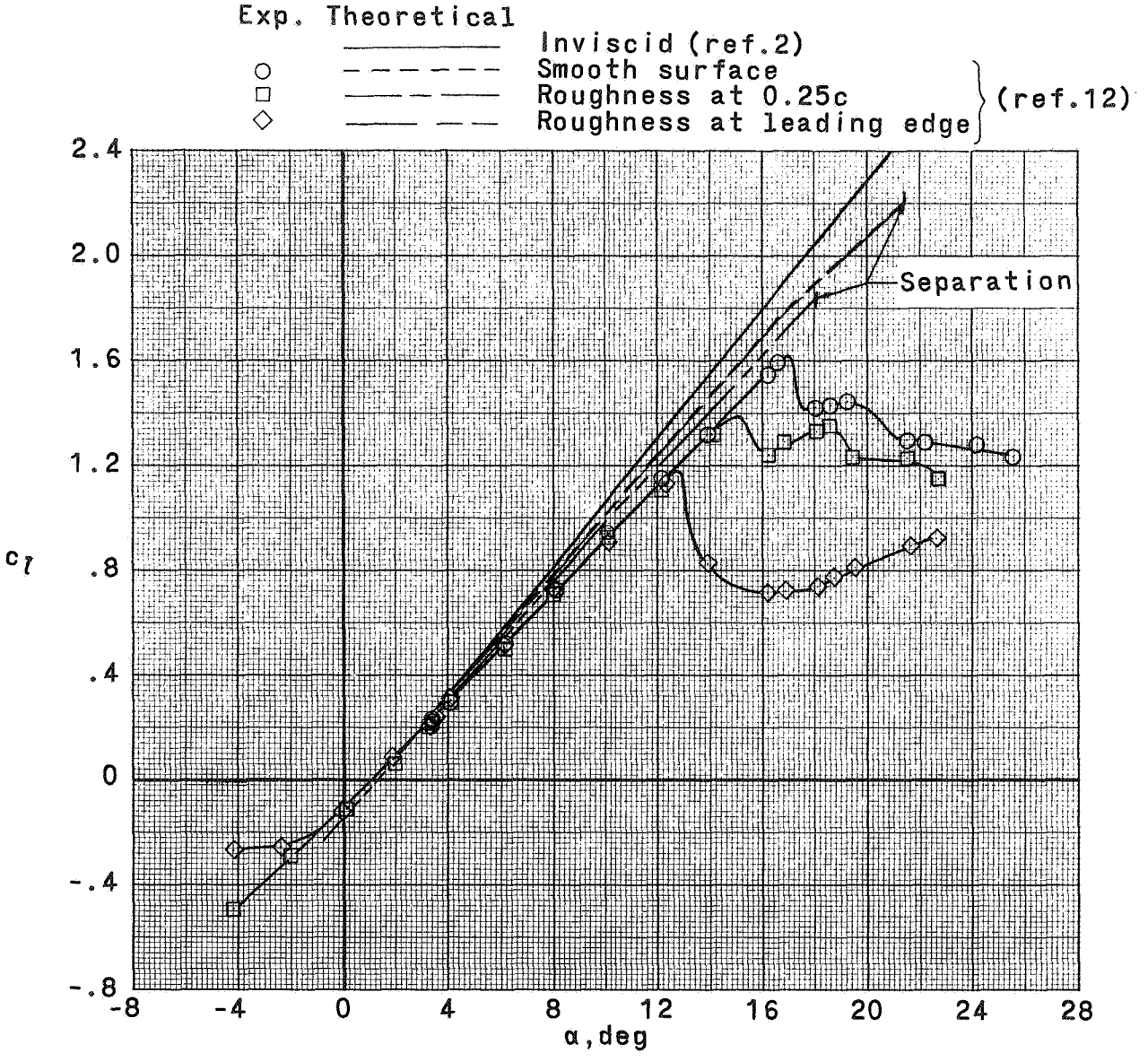

Figure 12.- Experimental and theoretical section lift coefficients.
$R \approx 9 \times 10^6$; $M = 0.1$.

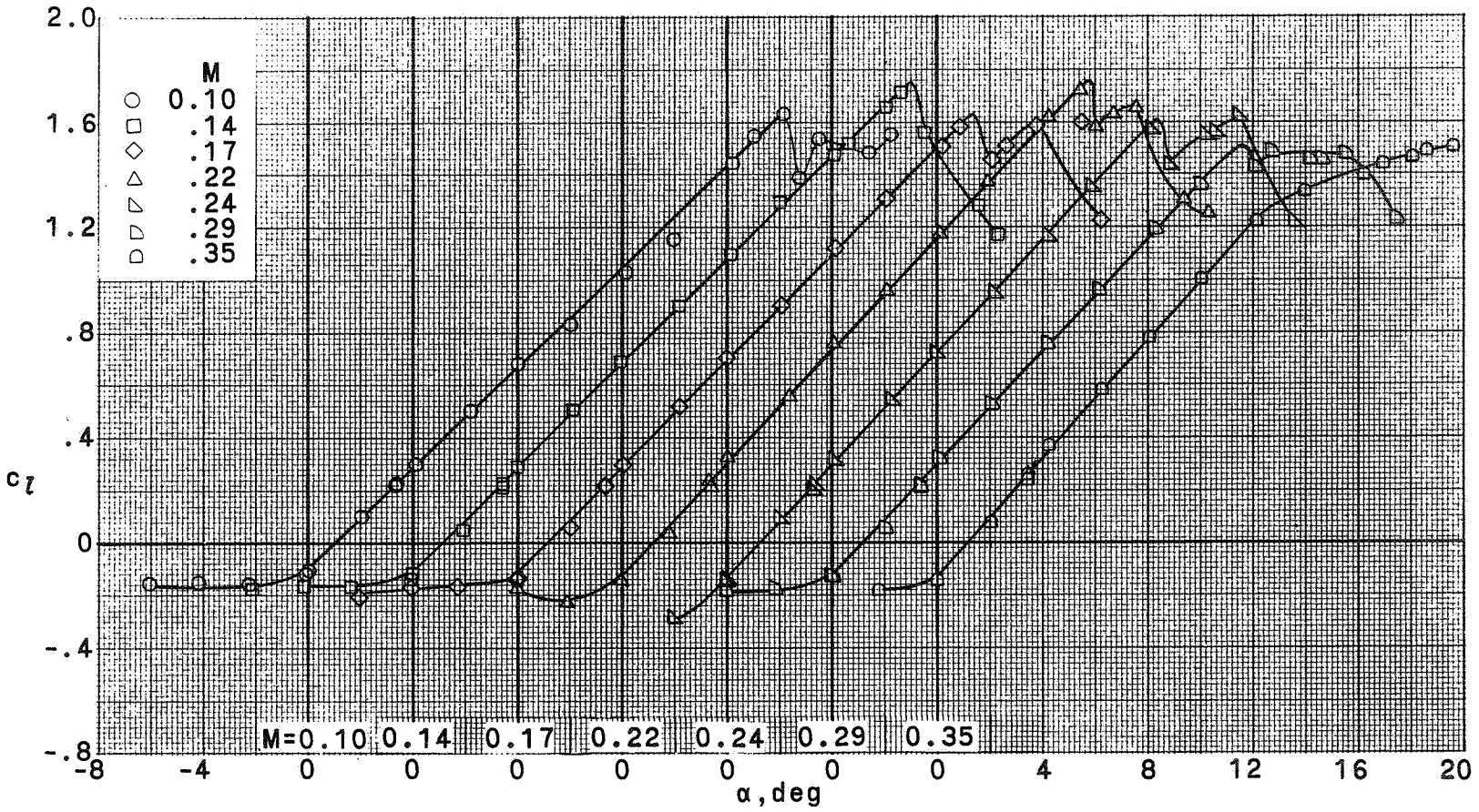

Figure 13.- Influence of Mach number on section lift coefficient. $R \approx 3.9 \times 10^6$; smooth surface.

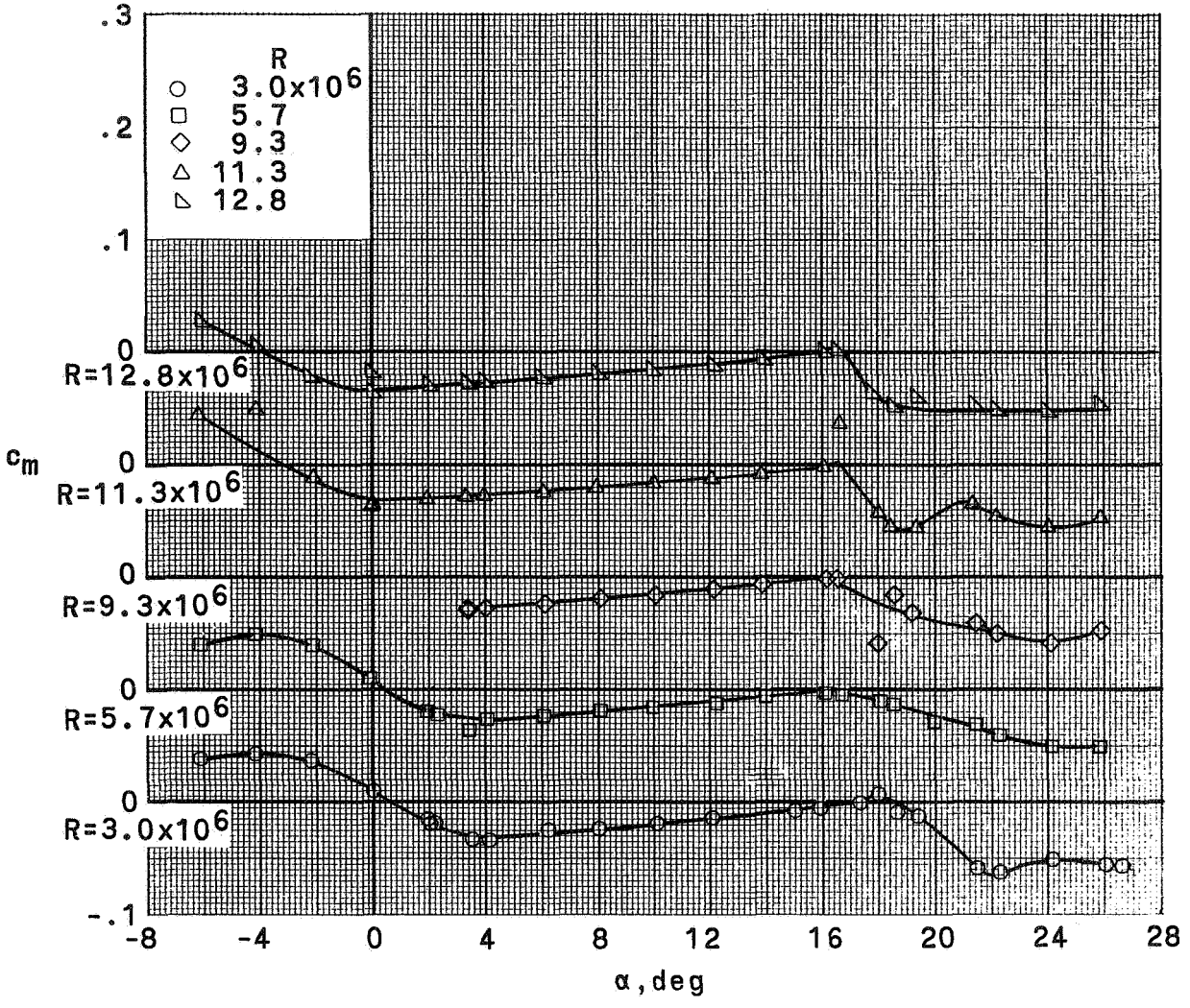

(a) Smooth surface.

Figure 14.- Influence of Reynolds number on section pitching-moment coefficient. M = 0.1.

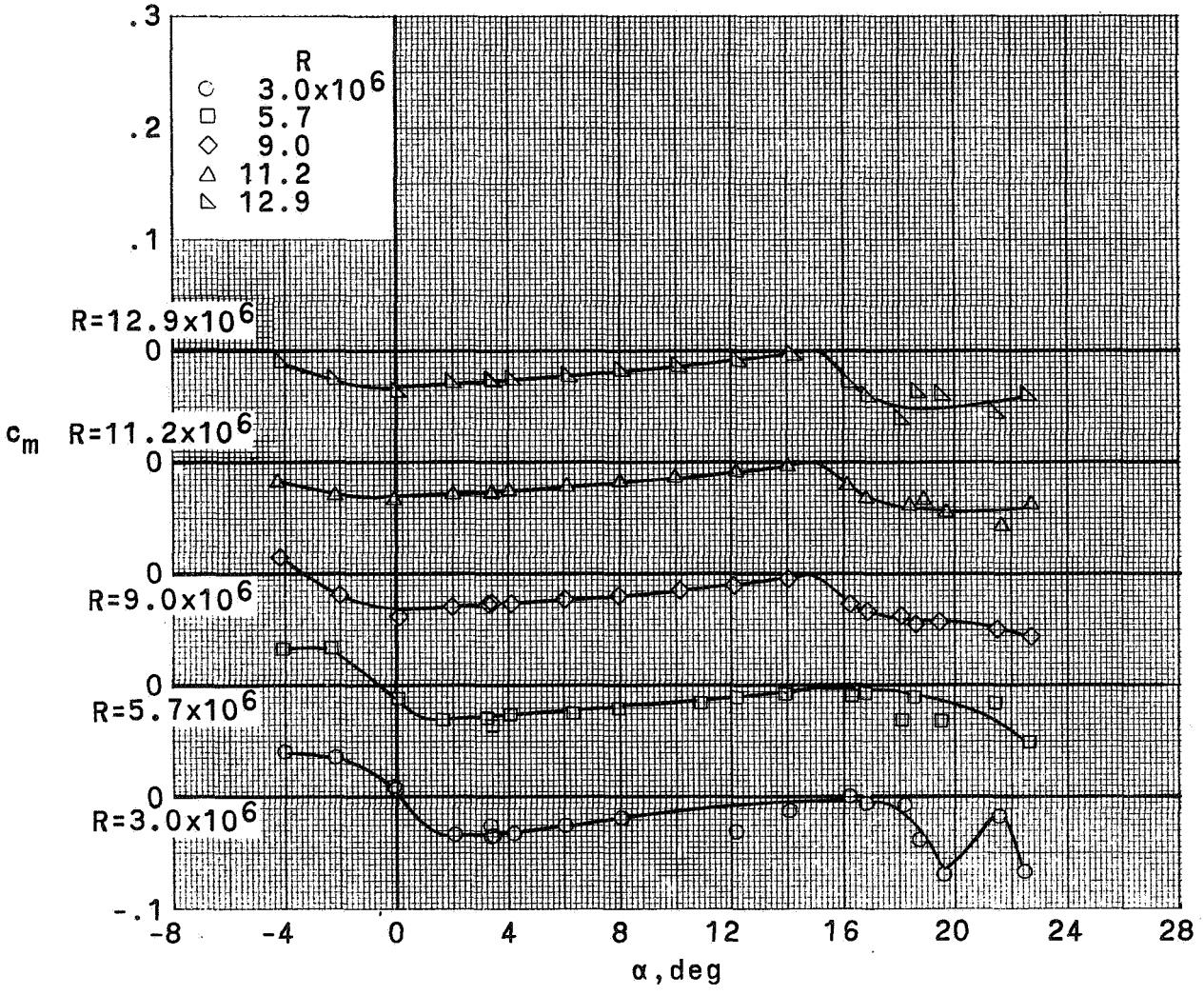

(b) Roughness at 0.25c on upper surface.

Figure 14.- Continued.

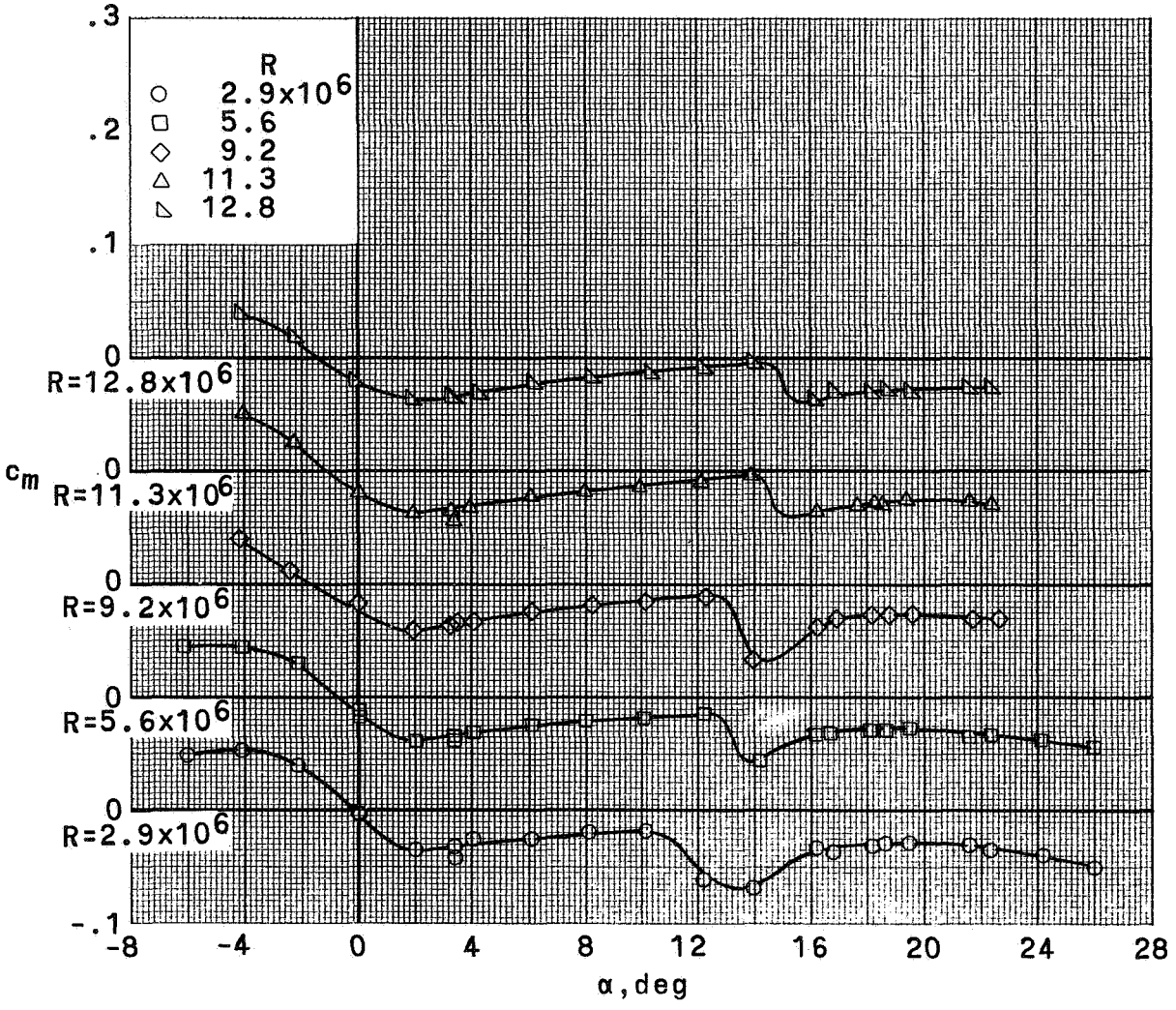

(c) Roughness at leading edge.

Figure 14.- Concluded.

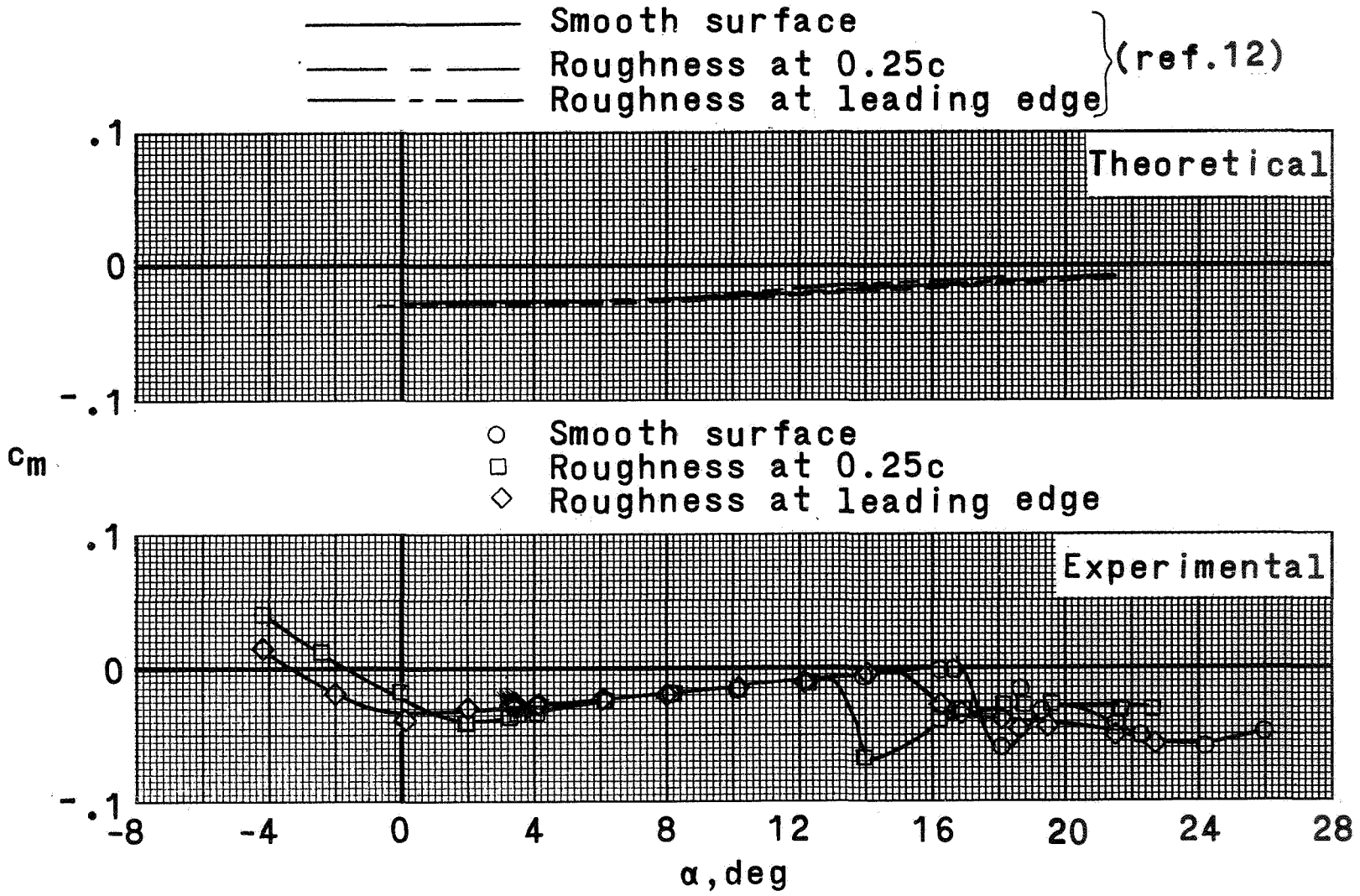

Figure 15.- Experimental and theoretical section pitching-moment coefficients. $R \approx 9.0 \times 10^6$; $M = 0.1$.

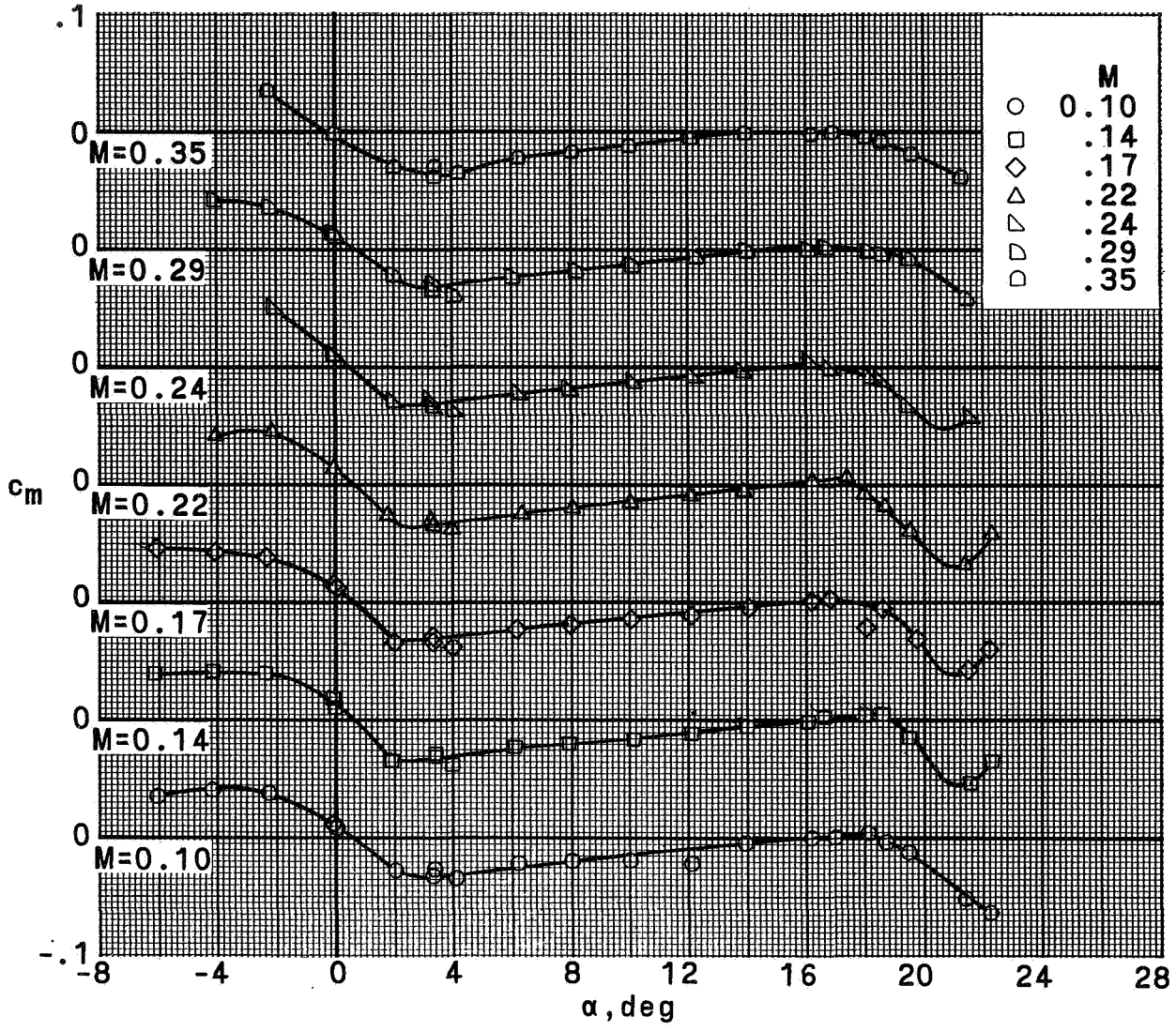

Figure 16.- Influence of Mach number on section pitching-moment coefficient. $R \approx 3.9 \times 10^6$; smooth surface.

NATIONAL AERONAUTICS AND SPACE ADMINISTRATION
WASHINGTON, D.C. 20546

OFFICIAL BUSINESS
PENALTY FOR PRIVATE USE $300

SPECIAL FOURTH-CLASS RATE BOOK

POSTAGE AND FEES PAID
NATIONAL AERONAUTICS AND SPACE ADMINISTRATION
451

U.S.MAIL

POSTMASTER: If Undeliverable (Section 158 Postal Manual) Do Not Return

"The aeronautical and space activities of the United States shall be conducted so as to contribute . . . to the expansion of human knowledge of phenomena in the atmosphere and space. The Administration shall provide for the widest practicable and appropriate dissemination of information concerning its activities and the results thereof."

—NATIONAL AERONAUTICS AND SPACE ACT OF 1958

NASA SCIENTIFIC AND TECHNICAL PUBLICATIONS

TECHNICAL REPORTS: Scientific and technical information considered important, complete, and a lasting contribution to existing knowledge.

TECHNICAL NOTES: Information less broad in scope but nevertheless of importance as a contribution to existing knowledge.

TECHNICAL MEMORANDUMS: Information receiving limited distribution because of preliminary data, security classification, or other reasons. Also includes conference proceedings with either limited or unlimited distribution.

CONTRACTOR REPORTS: Scientific and technical information generated under a NASA contract or grant and considered an important contribution to existing knowledge.

TECHNICAL TRANSLATIONS: Information published in a foreign language considered to merit NASA distribution in English.

SPECIAL PUBLICATIONS: Information derived from or of value to NASA activities. Publications include final reports of major projects, monographs, data compilations, handbooks, sourcebooks, and special bibliographies.

TECHNOLOGY UTILIZATION PUBLICATIONS: Information on technology used by NASA that may be of particular interest in commercial and other non-aerospace applications. Publications include Tech Briefs, Technology Utilization Reports and Technology Surveys.

Details on the availability of these publications may be obtained from:

SCIENTIFIC AND TECHNICAL INFORMATION OFFICE

NATIONAL AERONAUTICS AND SPACE ADMINISTRATION

Washington, D.C. 20546